ICARUS 122, 166–192 (1996)
ARTICLE NO. 0117

Synchronous Locking of Tidally Evolving Satellites

BRETT GLADMAN,* D. DANE QUINN,† PHILIP NICHOLSON,* AND RICHARD RAND†

*Department of Astronomy and †Department of Theoretical and Applied Mechanics, Cornell University, Ithaca, New York 14853
E-mail: gladman@astrosun.tn.cornell.edu

Received August 16, 1995; revised December 13, 1995

Satellite spin states evolve under the action of solid body torques and tidal forces. The tidal effects result in a damping of fast spin rates and, ultimately, in the locking of the spin into what are known as Cassini states. The dynamical equations for the satellite spin vector are derived, non-dimensionalized, and discussed. The non-dimensional parameters that determine the ultimate fate of the system are identified. A review of Cassini states is given, and then the effect of a permanent triaxial deformation on the evolution of the spin vector is explored. We find that for the parameter ranges of most real Solar System satellites which have been despun to synchronous rotation, occupation of Cassini state 1 is the only possible endpoint. The existence of a non-axially symmetric deformation destabilizes the higher obliquity Cassini state 2. We discuss the possibility of tumbling occurring during the spin-down and argue that this does not effect our basic conclusions. The non-occupancy of Cassini state 2 (except for the Moon, for which state 1 does not exist) is not a function of initial conditions or spin configuration occupied at synchronous lock, as previously hypothesized.

1. INTRODUCTION

In 1643 Cassini published his three laws on the motion of the Moon (see Colombo 1966) which, slightly rephrased, are:

1. The spin period is identical to the orbital period.
2. The spin axis maintains a constant inclination to the ecliptic plane.
3. The spin axis, orbit normal, and ecliptic normal remain coplanar.

The third of these implies that while the Moon's orbit precesses, its spin axis precesses at the same rate. The *spin axis precession* is caused by the small torque exerted by the Earth on the Moon's figure. The Moon is distant enough from the Earth that the *orbit precesses* about the ecliptic plane rather than the Earth's equatorial plane; this precession rate is a function of the orbital distance of the Moon and the mass of the Sun. Why should these two precession rates even be close, much less equal?

In general, consider a planetary satellite (see Fig. 1) whose circular orbit normal $\hat{\mathbf{K}}$ is inclined by an inclination i with respect to an invariable plane normal $\hat{\mathbf{n}}$, about which it precesses with a rate $-\mu$ (in rad/year). For close planetary satellites, the invariable plane is the planet's equatorial plane, and the orbit precession is caused by the oblateness of the planet. In general, the invariable plane is the satellite's Laplace plane in the three body system (Goldreich 1966a, Ward 1981). The satellite's spin angular momentum in the $\hat{\mathbf{k}}$ direction is tilted by an obliquity θ with respect to its orbit-plane normal $\hat{\mathbf{K}}$. If the satellite is oblate, the planet exerts a torque which attempts to cause a precession $\dot{\phi}$ of the spin axis about $\hat{\mathbf{K}}$. We will assume in what follows that the satellite is in principal-axis rotation about its axis of maximum moment of inertia. Averaged around the satellite's orbit, this torque is given by $-SC\cos\theta\sin\theta$, where C is the satellite's moment of inertia about the spin axis and

$$S = \frac{3Gm_p}{2r^3}\frac{C-(A+B)/2}{C}$$

is an angular acceleration (this expression is derived in Appendix A). In this expression m_p is the mass of the planet, G is the gravitational constant, r is the orbital radius of the satellite, and A and B are the other two principal moments of inertia. Because the orbit normal $\hat{\mathbf{K}}$ is not fixed, this torque actually causes $\hat{\mathbf{k}}$ to precess about $\hat{\mathbf{n}}$. Since the component of angular momentum perpendicular to $\hat{\mathbf{n}}$ is $Cw\sin(\theta-i)$, w being the (not necessarily synchronous) spin rate of the satellite, the solid body torque produces a precession rate about $\hat{\mathbf{n}}$ of

$$\dot{\Omega} = -\frac{S\sin\theta\cos\theta}{w\sin(\theta-i)}. \tag{1}$$

(If $\hat{\mathbf{k}}$ and $\hat{\mathbf{K}}$ were on the same side of $\hat{\mathbf{n}}$ in Fig. 1 then we would have $\sin(\theta+i)$ in the denominator instead.) The answer to the puzzle posed above is that tidal dissipation in the satellite drives it to a state where these two precession rates are equal; that is, the obliquity θ evolves to a point where

0019-1035/96 $18.00

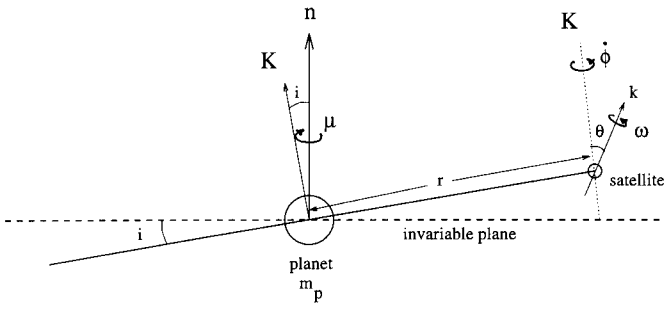

FIG. 1. Geometry of the problem. The orbital plane of the satellite, with normal **K**, precesses about the invariable plane normal **n** with a constant inclination i at an angular rate $-\mu$. The obliquity of the satellite's spin vector **k**, measured with respect to the orbit normal, is θ. Note that the azimuthal direction of the spin vector is suppressed in this cartoon. Torques exerted on the satellite's oblateness will cause **k** to precess about **n**. When this precession rate matches μ, the satellite is said to be in a generalized Cassini state.

$$\frac{S \sin\theta \cos\theta}{w \sin(\theta - i)} = \mu. \tag{2}$$

Such a satellite is said to be in a "generalized Cassini state," adopting Peale's (1969) usage. If one switches to a coordinate system fixed relative to the orbit plane that rotates uniformly with an angular velocity $-\mu$, then the spin axis of a satellite in a generalized Cassini state will appear stationary (though it is precessing in inertial space).

Depending on the ratio of $S/w\mu$, there can exist two or four values of the obliquity θ which satisfy (2) (see Section 3). For most planetary satellites, two of these Cassini states (denoted S_1 and S_2) seem to be stable end-states of tidal evolution (see Peale 1974). However, there are no satellites *for which both of these end-states exist* found in state S_2. (The Moon is the only satellite found in S_2; however, it has parameter values for which S_1 does not exist, leaving S_2 as the only possible Cassini state). Previously Peale (1974, 1977) speculated that the selection of state 1 or 2 might involve a probabilistic capture (which should be small for S_2), or a sudden shift of a separatrix when synchronous rotation is reached (which might push any satellite in S_2 out of that state). Kadano (1993) suggested that collisions are responsible for knocking satellites out of state 2 (the probability of going from S_2 to S_1 being much higher than the reverse). The question that we address here is: during the primordial spin-down, or any subsequent despinning event (after being struck by an impactor imparting a large amount of angular momentum, for example), what Cassini state will a planetary satellite evolve to? In particular, why do there not seem to be any satellites occupying the high obliquity Cassini state 2?

We first derive the orbit-averaged rotational equations of motion for a satellite, and convert the equations to a non-dimensionalized form in Section 2. The presentation of the paper then examines a progression of more complicated problems (each involving successively more terms in the equations of motion). Section 3 reviews the concept of generalized Cassini states. We then move on in Section 4 to discuss the more complete problem of the evolution of an oblate axisymmetric satellite under the action of tidal forces (the problem to which the most attention has been given in previous literature). We show that neglecting the triaxial shape of the satellite results in there usually being only one stable end-state, which is selected by the fixed parameters of the problem. In Section 5, we show that inclusion of the non-axisymmetric terms does not qualitatively alter this conclusion: only S_1 retains stability when both S_1 and S_2 exist, for physically plausible values of the parameters. Thus we conclude that all known synchronously locked planetary satellites could only be in state 1 (with the exception of the Moon).

2. THE EQUATIONS OF MOTION

2.1. *Variables and equations*

We consider a triaxial satellite in a circular, inclined, and precessing orbit about a planet, and in a state of principal-axis rotation (*i.e.*, the spin axis **k** is identical to the axis of maximum inertia). *The coordinate system is coprecessing* with the satellite's orbit plane. The satellite's rotational state is described by Euler angles θ, ϕ, ψ (see Fig. 15 in Appendix A), and its angular spin velocity w. Note that a triaxial body is symmetric under $\psi \rightarrow \psi + \pi$. Commonly used symbols are defined in Table I. As in Fig. 1, the obliquity θ is measured with respect to the instantaneous orbit normal **K**, which in turn is inclined at a constant angle i (the orbital inclination) relative to the invariable plane. The ascending node of the satellite's equator plane on its orbital plane is defined by the angle ϕ, while ψ locates the long axis of the satellite relative to this node.

We derive in Appendix A expressions for the rigid body and tidal torques and then the orbit-averaged, scalar equations of motion. The dynamical variable set is $(\omega, \theta, \phi, \psi_0)$, where $\omega \equiv w\mu/S$ is the dimensionless spin rate. Note from Eq. (1) that the spin axis precession rate due to the solid body torque on the satellite oblateness is $\dot{\Omega} \simeq -S \cos\theta/w$, if we neglect the orbital inclination. Thus, apart from geometrical factors, ω is essentially the ratio of the orbit and spin axis precession rates, $\mu/\dot{\Omega}$. For simplicity, we shall loosely refer to ω as the "spin rate", since it is proportional to the dimensional spin rate w. The variable ψ_0 measures the position of the long axis of the satellite relative to the planet, in the rotating frame. Defining f as the anomaly of the planet measured from the ascending node of the satellite's equator, then $\psi_0 = \psi - f$. Thus, in some sense,

TABLE I
Commonly Used Symbols

Symbol	Meaning
A	Satellite's moment of inertia about long axis
α	Solid body angular acceleration in dimensionless units
B	Satellite's moment of inertia about intermediate axis
β	Ratio of solid body torques ($B - A$ to oblateness)
C	Satellite's moment of inertia about the spin axis
ε	Fractional tidal despinning rate, in dimensionless units
f	Anomaly of planet in orbit plane, measured from **N**
G	Gravitational constant
γ	Synchronous rotation rate in dimensionless units
i	Inclination of satellite orbit (w.r.t. invariable plane)
K	Orbital normal
k	Satellite's spin axis
k_2	The tidal Love number of the satellite
n	Invariable plane normal
n	Satellite's mean motion
$-\mu$	Orbit precession rate
m_p	Planet mass
$\dot{\Omega}$	Spin precession rate from torque on satellite oblateness
ϕ	Euler angle locating equatorial and orbital line of nodes
ψ	Euler angle locating satellite's long axis
ψ_0	Angular position of A axis relative to planet, $\psi - f$
Q	Specific dissipation function of satellite
r	Radial distance of satellite from planet
R_s	The mean radius of the satellite
S	Spin axis precessional acceleration caused by torque on oblateness
S_n	Generalized Cassini state n
τ	Dimensionless time, μt. Derivatives w.r.t. τ are denoted by a superscript dot
θ	Spin obliquity, measured with respect to orbit normal
θ_{cr}	Critical value of obliquity above which S_2 is unstable in full problem
θ_n	Obliquity of Cassini state n
w	Spin rate, in dimensional units
ω	Spin rate, nondimensional, $\sim\mu/\dot{\Omega}$
ω_c	Critical spin rate where S_1/S_4 bifurcation occurs

when $\psi_0 = 0$ the long axis is as "aligned as much as possible" with the instantaneous direction to the planet (for $\theta = 0$ the long axis points directly at the planet when $\psi_0 = 0$). The interested reader is urged at this point to read Appendix A.

We find that the important ratios of various parameters that govern the behavior of the system are best seen if we non-dimensionalize the equations. The final equations of motion, averaged over one orbit *and* one spin period, are

$$\dot{\omega} = -\varepsilon\left[\omega\left(1 - \frac{1}{2}\sin^2\theta\right) - \gamma\cos\theta\right] - \beta(1 + \cos\theta)^2 \sin 2\psi_0 \tag{3}$$

$$\dot{\theta} = \sin i \sin\phi + \varepsilon \sin\theta\left[\frac{1}{2}\cos\theta - \frac{\gamma}{\omega}\right] + \frac{\beta}{\omega}\sin\theta(1 + \cos\theta)\sin 2\psi_0 \tag{4}$$

$$\dot{\phi} = \sin i \cot\theta \cos\phi + \cos i - \frac{1}{\omega}\cos\theta - \frac{\beta}{\omega}(1 + \cos\theta)\cos 2\psi_0 \tag{5}$$

$$\dot{\psi}_0 = \alpha(\omega - \gamma), \tag{6}$$

where the dot denotes differentiation with respect to the dimensionless time variable τ.

In the dimensionless system the unit of time is $1/\mu$ so that all time scales are relative to the orbital precession period (which is 2π). In these equations the three terms involving the orbital inclination result from the precession of the coordinate system. The $(-1/\omega)$ term in the $\dot{\phi}$ equation is the precession induced by the torque on the satellite's oblateness. Terms due to the tidal dissipation involve the small quantity $\varepsilon(\ll 1)$, which is the fractional amount by which the satellite is tidally despun in one time unit, while terms of order $\beta(\sim 1)$ are caused by the triaxial shape of the body, and will average out for non-synchronous rotation. γ is just the value of ω when the satellite is in synchronous rotation. The fourth equation links the orientation angle ψ_0 to the dimensionless spin and orbital rates. The quantity $\alpha(\gg 1)$ is the solid body angular acceleration S (due to the satellite oblateness) expressed in the new time units. α is very much larger than unity for planetary satellites for the simple reason that the precessional period is always much longer than the orbital period (see Eq. (7)). Thus only when ω is very close to γ does the rate of change of ψ_0 slow down and prevent the β terms from averaging to zero. For rotation rates much above synchronous we can effectively ignore the β terms.

The parameters α, β, and γ can be expressed as simple combinations of the moments, the mean motion n, and the orbit precession rate:

$$\alpha = \frac{3}{2}\left(\frac{n}{\mu}\right)^2\left[\frac{C - (A + B)/2}{C}\right]$$

$$\beta = \frac{1}{4}\left[\frac{B - A}{C - (A + B)/2}\right] \tag{7}$$

$$\gamma = \frac{2}{3}\left(\frac{\mu}{n}\right)\left[\frac{C}{C - (A + B)/2}\right].$$

Specifying these three parameters is equivalent to giving the three ratios A/C, B/C, and μ/n. α is proportional to

the oblateness of the satellite, but contains the ratio of the orbital motion to its precession. β is simply the ratio of the two triaxial asymmetries, but is also the ratio of the non-axisymmetric solid body torque to the axisymmetric torque, so for an axisymmetric body, $\beta = 0$. We shall see later that the fundamental parameter that governs the spin evolution is $\gamma \equiv \mu n/S$ (*i.e.*, $\mu/\dot{\Omega}$ when the satellite is in synchronous rotation, to within geometrical factors). When the dimensionless spin rate ω is reduced to γ the satellite's spin has reached the synchronous state (*cf.* Eq. (6)). By (7) we see that the only way γ can exceed unity is for the moment differences to be very small, or for the orbit precession to be very rapid. Since $\mu \ll n$, it is probably true that $\gamma \ll 1$ for all planetary satellites except for very distant or very spherical ones, the Moon being an excellent example. In this case, due to solar torques, $\mu/n \simeq 0.004$, while $[C - (A + B)/2]/C \simeq 5 \times 10^{-4}$, leading to $\gamma \simeq 5$. For Mimas (which is more typical) $\mu/n \simeq 0.003$ while $[C - (A + B)/2]/C \simeq 0.057$, so that $\gamma \simeq 0.032$.

2.2. *Parameter Values*

The measurements required to determine the values of the dimensionless parameters for planetary satellites are unfortunately scarce. This is especially true for the moment differences, which are known only for the Moon (Yoder 1995). The moments of Phobos and Deimos are calculated from Viking images by Rubincam, *et al.* (1995). From spacecraft encounters we know the shapes of six other satellites sufficiently well that we can calculate moment differences directly from their ellipsoidal shapes (as given by Dermott and Thomas 1988, Thomas 1988, Thomas 1990, and Thomas and Dermott 1991). That is, if $a > b > c$ are the satellite's principal-axial radii, then we have

$$\frac{B - A}{C} = \frac{a^2 - b^2}{a^2 + b^2},$$

$$\frac{C - (A + B)/2}{C} = \frac{(a^2 + b^2)/2 - c^2}{a^2 + b^2}.$$

The parameters α, β, and γ can thus be calculated from this information and the known periods and precession rates (see Table II). As we shall see, γ is really the most important of these, and we will show that our results about the stability of the Cassini end states are insensitive to errors in α and β of less than an order of magnitude. The nodal precession rates μ are simply calculated from the planetary values of J_2, except for the Moon, which is dominated by solar perturbations (Goldreich 1966b), and whose precession rate is measured (see Yoder 1995).

We offer one cautionary note regarding the values of β. The present values given in Table II are probably larger than the unknown values that applied during the primordial spin-down phase. Once synchronously locked, the satellites will tend to deform to hydrostatic shapes that conform to the tidal gravitational field exerted by the primary, for which $\beta = 3/10$. Dermott and Thomas (1988) conclude that this has happened to Mimas, and the fact that the shapes of many satellites can be fit well by equilibrium ellipsoids lends support to this hypothesis. Jankowski *et al.* (1989) tabulate moment differences, under the assumption of hydrostatic shapes, for all the regular satellites. Even for the Moon, Phobos, and Deimos, however, which are known not to have hydrostatic shapes, β is within a factor of 3 of 0.3. Thus the primordial values of β were probably not less than 1/3 to 1/10 of the values given here. We shall show that even reducing β by an order of magnitude will not alter our conclusions.

TABLE II
Parameter Values for a Selection of Satellites

Object	μ(°/day)	i(°)	α	β	γ	ε
Moon	0.054	5.1	4.5×10^{1}	0.11	5.3259	2×10^{-5}
Deimos	0.018	1.8	7.7×10^{7}	0.29	0.0002	2×10^{-6}
Phobos	0.436	1.9	2.1×10^{6}	0.14	0.0012	1×10^{-5}
Io	0.133	0.03	1.8×10^{4}	0.29	0.0839	1×10^{-2}
Mimas	1.000	1.6	1.2×10^{4}	0.29	0.0322	3×10^{-4}
Enceladus	0.415	0.02	1.7×10^{4}	0.32	0.0371	4×10^{-4}
Tethys	0.198	1.1	1.4×10^{4}	0.39	0.0682	1×10^{-3}
Miranda	0.056	4.2	5.8×10^{5}	0.35	0.0079	2×10^{-3}
Ariel	0.017	0.04	3.5×10^{5}	0.44	0.0250	9×10^{-3}

The tidal despinning parameter ε is subject to much greater uncertainty. In terms of the usual tidal dissipation factor Q, the tidal phase lag $2(w - n)\Delta t \simeq 1/Q$ (Goldreich and Peale 1970). Except for the Moon for which the ratio $k_2/Q = 0.0011$ is available (Dickey *et al.* 1994), we have arbitrarily chosen Δt so that $Q = 100$ at a tidal frequency $2(w - n) = n$. For the Love number k_2 we use

$$k_2 = \frac{3/2}{1 + 19\mu^*/(2\bar{\rho}gR_s)}$$

(Burns 1977) where $g = Gm_s/R_s^2$ is the surface gravity of the satellite, $\bar{\rho}$ is its mean density, and the rigidity μ^* is taken to be 3×10^{11} dyn/cm^2 for rocky objects, and 4×10^{10} dyn/cm^2 for icy ones. The densities of Mimas, Enceladus, Tethys, Ariel, and Miranda were taken to be 1.2 g/cm^3; for Io we used $\bar{\rho} = 3.5$ g/cm^3. For most satellites $k_2 \ll 1$, and we have

$$\varepsilon \simeq \frac{45\bar{\rho}R_s^2 n^3}{19\mu^*\mu Q}.$$

Since for most satellites the orbit precession rate $\mu \propto J_2 r^{-7/2} \propto J_2 n^{7/3}$, ε scales only as r^{-1}, and thus can be somewhat greater for a distant, large satellite than a close,

smaller one (compare Mimas and Tethys, or Miranda and Ariel, in Table II). Since $\varepsilon \ll 1$, the exact value of this parameter will make little difference to the stability of the endpoints, and affects only the rate of evolution to those states. Therefore the likely order of magnitude uncertainty in the actual value of Q used here is of little concern.

2.3. *Review of Approximations*

Before we proceed, we review the assumptions involved in our approach. A circular orbit is assumed for the satellite; a non-circular orbit will induce periodic behavior in the amplitude of the rigid body torques. One classic effect of this is to allow the possibility of capture of the satellite into a non-synchronous spin–orbit resonance, as in the case of Mercury (Goldreich and Peale 1966). For the low eccentricities of planetary satellites this capture probability is small, and apparently did not happen. An eccentric orbit for the satellite also would allow for chaotic tumbling, the possibility of which is discussed below. Tidal effects tend to circularize satellite orbits in any case, although the time scale for such orbital evolution is generally longer than that necessary to damp the spin rate. We also neglect semimajor axis evolution, since this occurs on an even longer time scale.

The most serious approximation is our assumption of principal-axis rotation. This approximation permits us to average the equations of motion over both the orbital and spin periods. A satellite struck by a large impactor will usually have a wobble (non-principal-axis rotation) component introduced into its spin. The wobble decay times (see Burns and Safronov 1973, Harris 1994) of planetary satellites can be comparable to their spin-down times. The relevant time constants are given by Peale (1977),

$$\tau_{\text{wobble}} = \frac{3GCQ}{w^3 k_2 R_s^5} \tag{8}$$

$$\tau_{\text{despin}} = \frac{wr^6 CQ}{3Gm_p^2 k_2 R_s^5}, \tag{9}$$

where the symbols are defined in Table I. The ratio of the wobble decay to despinning time scale $\tau_w/\tau_d = 9(n/w)^4$, and thus any satellite that is initially spinning much faster than twice synchronous will have its wobble damped on a time scale negligible compared to its spin-down time. A full study of the spin-down of a satellite including non-principal-axis rotation is beyond our computational abilities since it would require the ability to encompass the sub-orbital, precessional, and tidal time scales in a single numerical calculation while directly computing all of the torques.

The restriction to principal-axis rotation might be seen as unjustified in light of Wisdom (1987), who observes that irregular planetary satellites can be induced to tumble as the satellite switches from having its long axis circulating to librating (in the co-rotating reference frame). Beletskii (1972) showed that in the obliquity range $\theta \simeq 58°$–$97°$ triaxial satellites near synchronous rotation are subject to wobble instabilities. We will discuss this point further after we present the results of our study of non-axisymmetric satellites, where we argue that this effect, although almost certainly present, does not affect our conclusions regarding the ultimate stability of the Cassini states.

3. REVIEW OF CASSINI STATES

In the absence of tidal dissipation (*i.e.*, $\varepsilon = 0$) Eqs. (3)–(6) describe the precession of the satellite in the rotating frame. The dynamics are discussed by Henrard and Murigande (1987), Peale (1977), and Beletskii (1972); we simply review the principal results in the setting of our dimensionless equations (which make the behavior fairly transparent).

3.1. *Axisymmetric Satellites*

Consider first the case of an axisymmetric satellite ($\beta = 0$) on which no tidal forces act ($\varepsilon = 0$). (Alternately consider watching a non-synchronous satellite on a time scale much shorter than that over which tides can affect the spin vector). The ψ_0 variable becomes irrelevant, and we are left with the reduced set of dimensionless equations

$$\begin{aligned} \dot{\omega} &= 0 \\ \dot{\theta} &= \sin i \sin \phi \\ \dot{\phi} &= \sin i \cot \theta \cos \phi + \cos i - \frac{1}{\omega} \cos \theta. \end{aligned} \tag{10}$$

Not surprisingly, without dissipation the spin rate ω is constant. We can thus think of the spin rate ω as a parameter, and the trajectories describe paths in $(\theta, \phi) \subset S^2$ on the surface of a sphere. Note that γ (and hence the mean motion n) does not appear in these equations, so there is nothing special about synchronous rotation.

The terms that do not involve ω simply describe the *apparent* motion of the spin vector in the orbital frame due to the precession of the coordinate axes. As a trivial case, if the satellite is spherical so that $\omega \to \infty$ and the orbital inclination $i = 0$ then the obliquity θ is constant and the spin axis' azimuthal precession rate is unity, *i.e.*, the spin vector appears to precess at constant obliquity at the same rate as the coordinate system (recall that the orbital precession rate μ defines the non-dimensional time scale).

For an oblate satellite the torque exerted on the equatorial bulge modifies this simple solution. The resulting pre-

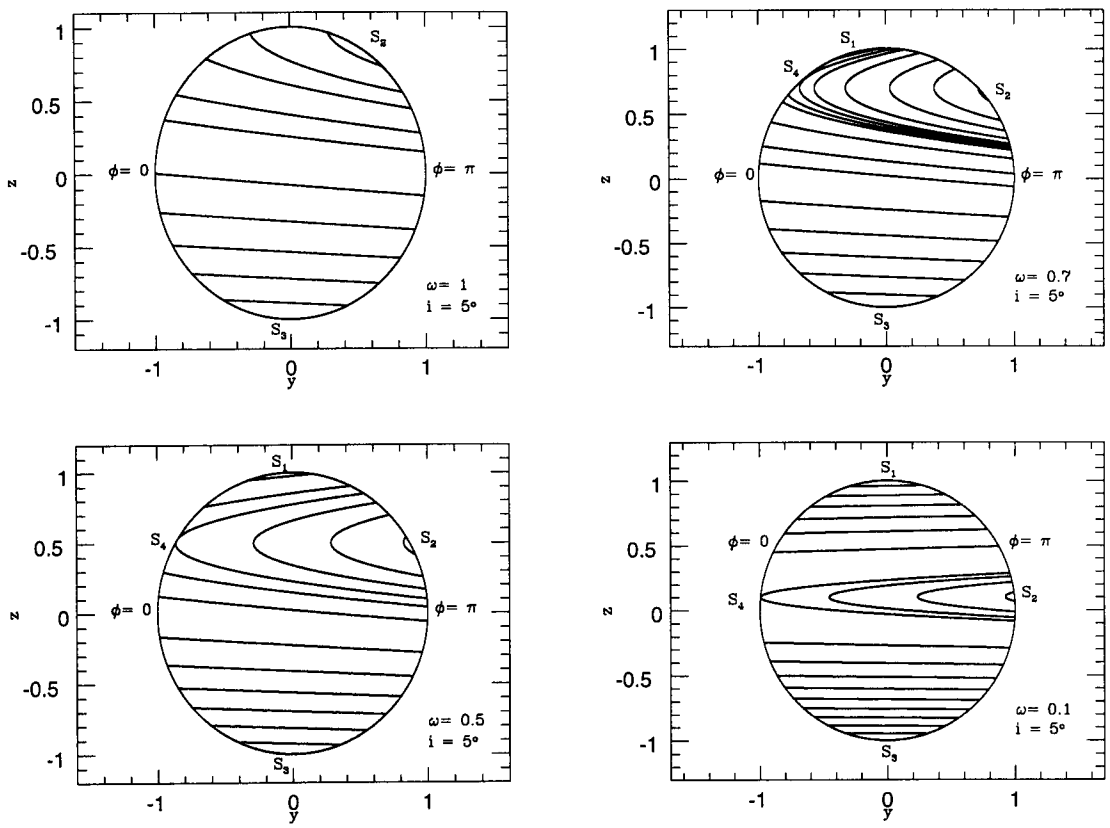

FIG. 2. Precession trajectories for the Cassini problem. These panels show the level sets of the Cassini Hamiltonian (11) projected onto the unit sphere, and thus the paths traced out by the spin axis of an axisymmetric satellite in the rotating coordinate system, for various values of the (fixed) dimensionless parameter ω. At any given value of ω, there are values of the Hamiltonian such that the vertices of the parabolic sheets do not intersect the sphere. The transformation $(\sin\theta\sin\phi, -\sin\theta\cos\phi, \cos\theta) \rightarrow (X, Y, Z)$ is used. The diagrams are relatively insensitive to the value of the orbit inclination for $i < 10°$, except very close to the critical value of ω where S_1 and S_4 appear (see the discussion in the text). The locations of the generalized Cassini states (where there is no precession in the rotating frame) are shown.

cession trajectories are closed because Eqs. (10) are derivable from the Hamiltonian,

$$H = \sin i \cos\phi\sqrt{1-\cos^2\theta} - \cos\theta\cos i + \frac{\cos^2\theta}{2\omega}, \quad (11)$$

where ϕ and $\cos\theta$ are the canonically conjugate coordinates. The advantage of this representation is that we immediately realize that the trajectories are just the level set of the Hamiltonian on the unit sphere. A manifold of constant H is a parabolic sheet that intersects the unit sphere along a curve that is one of the precession trajectories. Examples are shown in Fig. 2, for several values of ω. We see that there are up to four special values for the Hamiltonian, at which the parabolic sheet is tangent to the sphere (and thus we have a fixed point of the equations of motion). These are the *generalized Cassini states*, as introduced by Colombo (1966) and Peale (1969), and are by convention numbered S_1 through S_4 as shown. One can examine an orthogonal view of this sphere to get a better view of three of the four generalized Cassini states, as shown in Fig. 3. State 4 is a saddle point of the flow, and the two homoclinic trajectories that pass through it separate trajectories circulating around S_1, S_2, and S_3, which are centers. S_2 is on the opposite hemisphere and thus cannot be seen in Fig. 3. They are referred to as "generalized" because the first of Cassini's laws (synchronous rotation) is not necessarily obeyed. In general there is nothing special about the satellite's rotational orientation relative to the planet while in a generalized Cassini state; it is not true that a single hemisphere faces the primary for example. However, S_1, S_2, and S_3 are the libration centers around which the spin vector of a non-synchronously rotating satellite will precess on time scales over which tides are negligible. We shall see that tidal effects will eventually drive the satellite to a true synchronous Cassini state, but the concept of the generalized, non-synchronous Cassini state is a useful one. Often we will drop the word 'generalized' in what follows, assuming it to be understood.

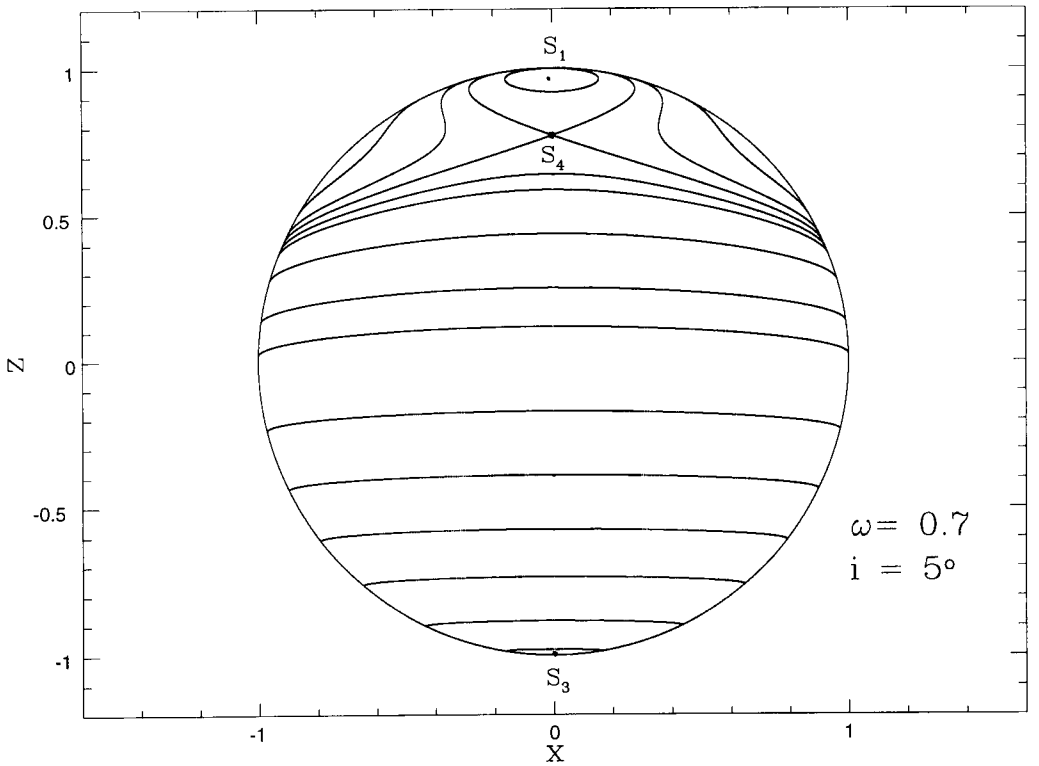

FIG. 3. This figure shows the $\phi = 0$ side of the unit sphere ($\phi = 0$ along $X = 0$ in this projection), corresponding to the $\omega = 0.7$ panel of Fig. 2. The separatrix through state S_4 is more clearly visible. S_2 is on the reverse side of this sphere.

The locations of the Cassini states can be easily obtained from Eqs. (10). For a fixed point we clearly must have $\sin\phi = 0 \Rightarrow \phi = 0$ or π. The $\dot{\phi}$ equation then furnishes the equation for the required value of θ,

$$0 = \sin i \cos\theta \cos\phi + \cos i \sin\theta - \frac{1}{\omega}\cos\theta \sin\theta$$
$$\Rightarrow \sin(\theta \pm i) = \frac{1}{2\omega}\sin(2\theta), \tag{12}$$

where if $\phi = (0, \pi)$ then we take the $(+, -)$ sign, respectively. The $\phi = \pi$ case recovers condition (2) for co-precession of the spin axis and orbit normal in Fig. 1. For $\phi = \pi$ there is always a single solution to this equation on $\theta \in [0, \pi]$; this is the location of Cassini state S_2. For $\phi = 0$ there are three solutions if $\omega < \omega_c$, a critical value which depends on the orbital inclination, or only one solution (S_3) if $\omega > \omega_c$. As ω decreases through $\omega = \omega_c$ a saddle-node bifurcation occurs, creating states S_1 and S_4 (Fig. 2). The critical value for the spin at which the bifurcation occurs is a function only of the orbit inclination, and a plot of ω_c vs i is given in Fig. 4a.

The highest obliquity state for $\phi = 0$ is always S_3, while if the other two states exist, S_1 is the lower obliquity of the two and S_4 is of intermediate obliquity. This is illustrated in Fig. 4b, which shows a bifurcation diagram (a plot of the locations of the equilibrium points as a function of a tunable parameter, in this case ω) for the obliquities θ of the Cassini states as a function of ω for an inclination $i = 5°$. For rapid orbital precession relative to spin axis precession ($\omega \gg \omega_c$), the two possible Cassini states asymptotically approach $\theta = i$ for S_2, and $\theta = \pi - i$ for S_3; that is, aligned and anti-aligned with the normal to the invariable plane $\hat{\mathbf{n}}$. The Moon falls into this category, with $i \simeq 5.1°$ and $\theta_2 \simeq 6.7°$. For slow orbital precession ($\omega \ll \omega_c$), which is the case for almost all other regular satellites, the four Cassini states approach ($\theta = \pi/2$, $\phi = \pi$) for S_2 and ($\theta = 0, \pi/2, \pi$; $\phi = 0$) for S_1, S_4, S_3, as in the last panel of Fig. 2. Specifically, when ω is small, the commonly occupied state S_1 lies at $\theta_1 \simeq \omega \sin i$ (see Eq. 12). This is the situation for most (and possibly all) other despun satellites. Note that when looking at Fig. 4b one should not think that the S_2 and S_4 branches are in any sense "close," as they are π radians apart in ϕ.

3.2. *Triaxial Satellites*

The above results hold only for axisymmetric satellites, or those that are not near synchronous rotation. For a

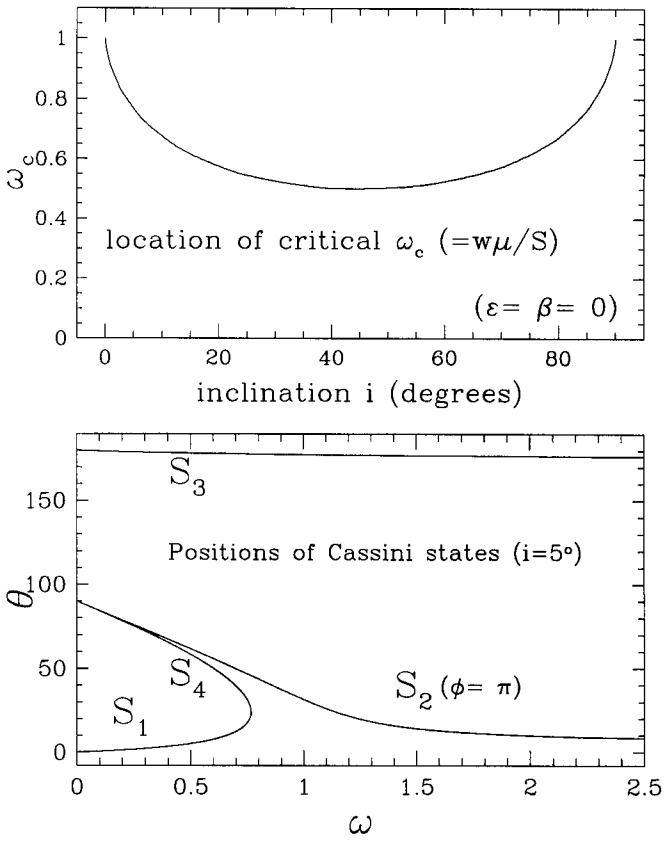

FIG. 4. Properties of the Cassini state problem, in which the spin rate ω is fixed. (top) For high spin rates there are only two fixed points of the Cassini state equation (12). This plot shows the value of ω_c below which there are four Cassini states instead of two. For small i, which is typical for planetary satellites, $\omega_c \simeq 1$. (bottom) Obliquities of the Cassini states for $i = 5°$ (for smaller inclinations the plot changes very little). The Cassini state obliquities depend on the value of ω. Note that the S_1/S_4 saddle-node bifurcation occurs at $\omega \simeq 0.8$, as expected from the upper plot. $\phi = 0$ for all branches except S_2, for which $\phi = \pi$; the S_2 and S_4 branches are thus not in any sense close to each other.

triaxial satellite close to synchronous rotation, the positions of the Cassini states (which now obey all three of Cassini's laws) shift. For ψ_0 = constant, we require $\omega = \gamma$ and examine the fixed points of the system:

$$\dot{\omega} = -\beta(1 + \cos\theta)^2 \sin 2\psi_0 \tag{13}$$

$$\dot{\theta} = \sin i \sin\phi + \frac{\beta}{\omega} \sin\theta (1 + \cos\theta) \sin 2\psi_0 \tag{14}$$

$$\dot{\phi} = \sin i \cot\theta \cos\phi + \cos i - \frac{1}{\omega}\cos\theta$$

$$- \frac{\beta}{\omega}(1 + \cos\theta)\cos 2\psi_0. \tag{15}$$

(If the satellite is close to, but not exactly in, synchronous rotation, the fast libration that results for the ψ_0 variable (see Section 5) effectively results in the average value of ω being γ.) Now, (13) implies that $\psi_0 = m\pi/2$, where m = 0, 1, 2, 3, but because of instabilities explained in Section 5, we need only consider $\psi_0 = 0$ or π. Thus (14) again implies that $\phi = 0$ or π, and we recover the usual expression for the obliquities of the Cassini states of a synchronous triaxial satellite (Peale 1977):

$$\sin(\theta \pm i) = \frac{1}{2\omega}\sin(2\theta) + \frac{\beta}{\omega}\sin\theta(1 + \cos\theta). \tag{16}$$

Again there are two solutions for $\omega \gg 1$ and four for $\omega \ll 1$, which are numbered in the same fashion as before. A small displacement from S_1, S_2, or S_3 (for a satellite unaffected by tidal forces) results in the pole precessing about the fixed point. We will discuss the stability of these states to tidal perturbations in Section 5.2. For synchronous bodies, the precession trajectories on the sphere are again determined by the intersections with a parabolic surface (see Peale 1977). Observe that even for a triaxial body, the full Cassini states will only become the precession centers near synchronous rotation; until $\omega \simeq \gamma$ the sin $2\psi_0$ and cos $2\psi_0$ terms rapidly average to zero, and the body will precess around a generalized Cassini state. Generalized Cassini states exist for all values of ω at particular values of the spin obliquity. The Cassini states (generalized or not) would thus seem to be mostly a curiosity, near which satellites would be found only by chance, were it not for the fact that they are closely related to the natural endpoints of tidal evolution for a precessing orbit.

4. EVOLUTION OF AXISYMMETRIC SATELLITES

4.1. Fixed Orbit

Consider an oblate, axisymmetric satellite in a *fixed* (non-precessing) orbit. It is easy to show from the dimensional equations of motion in Appendix A that there is only one, globally asymptotically stable, fixed point, corresponding to synchronous rotation with zero obliquity. The time scale for the decay is just the classic despinning time (see Eq. (9)). However, low obliquity satellites with $w > 2n$ are initially driven *away* from zero obliquity, as was noted by Darwin (1879) and Goldreich and Peale (1970). Peale (1977) explains this effect in terms of the torques on the components of the angular momentum vector. Also note that satellites beginning with retrograde rotations (cos $\theta < 0$) can temporarily be driven sub-synchronous. Regardless of these interesting detours, the final state is always $\theta = 0$, $w = n$.

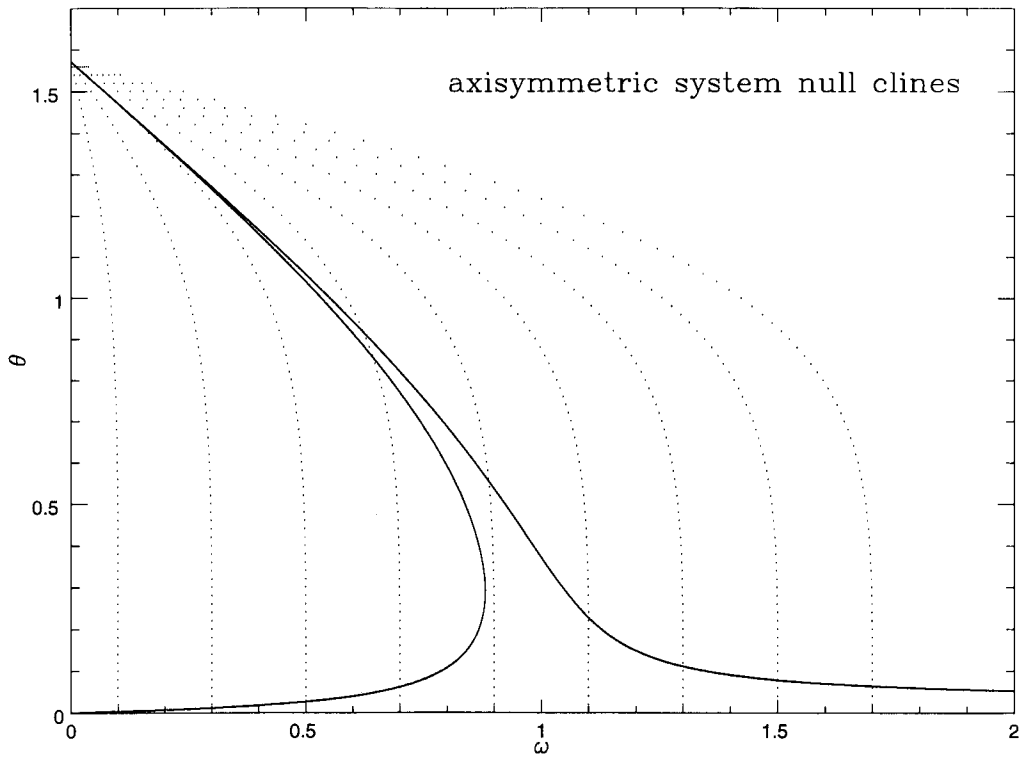

FIG. 5. Null clines of the axisymmetric system. The solid line is the null cline of the $\dot{\theta}$ and $\dot{\phi}$ equations projected onto the θ, ω plane, for the parameter values of Mimas. The solid S_2/S_4 null cline does not extend all the way to $\omega = 0$, but in fact stops at $\omega \simeq 4 \times 10^{-4}$ due to the new saddle-node bifurcation. The dotted lines show the null clines of the $\dot{\omega}$ equation, for various values of γ (the value of γ simply being the value of ω at which the null cline intersects the ω axis). All the $\dot{\omega}$ null clines have $\theta \to \pi/2$ *as* $\omega \to 0$.

4.2. Precessing Orbits

Before analyzing the full four-dimensional equations we consider the behavior of an axisymmetric satellite ($\beta = 0$) in a precessing orbit, evolving under the influence of tidal forces. Equation (6), governing ψ_0, decouples when $\beta = 0$, reducing Eqs. (3)–(6) to what we call the *axisymmetric system*:

$$\dot{\omega} = -\varepsilon \left\{ \omega \left(1 - \frac{\sin^2 \theta}{2} \right) - \gamma \cos \theta \right\},$$

$$\dot{\theta} = \sin i \sin \phi + \varepsilon \sin \theta \left\{ \frac{\cos \theta}{2} - \frac{\gamma}{\omega} \right\}, \qquad (17)$$

$$\dot{\phi} = \sin i \cos \phi \frac{\cos \theta}{\sin \theta} + \cos i - \frac{\cos \theta}{\omega}.$$

Recall that the tidal dissipation rate ε satisfies $0 < \varepsilon \ll 1$. Our $\beta = 0$ restriction is not as artificial as it may appear, since this set of equations applies even to triaxial satellites in an average sense as long as the rotation rate does not closely approach the synchronous value ($\omega = \gamma$).

In contrast to the analysis of Cassini states in Section 3, the spin rate ω is no longer a parameter of the system. Instead, ω is now a variable, coupled to the position of the spin axis. In addition, γ (and thus the mean motion n) now appears as a parameter in the system. From numerical integrations of Eqs. (17) we have found that the final state and qualitative behavior of the system are determined almost completely by γ; changes in either the tidal damping rate ε or inclination i do not dramatically alter the tidally evolved endpoints of the axisymmetric satellite for realistic ranges of these parameters.

At this point, our approach differs qualitatively from that of Peale (1974), who studied the tidal evolution of Mercury into a Cassini state. Peale's approach was to ignore the $\dot{\omega}$ equation and numerically integrate the remaining system around one precessional cycle, during which the spin rate of the satellite will change only very slightly. Since the position of the Cassini states will not change if the spin rate ω is constant (Fig. 4), over a single precession the Cassini state position (and hence the precession trajectory) is fixed. Thus Peale examined the sense of drift of the obliquity θ, numerically integrated over a single precession trajectory, a full numerical integration being prohibitive at the time. He presented his results of the

form of plots of the averaged rate of drift of the obliquity $\langle\dot{\theta}\rangle$ as functions of θ, for various values of $\omega/\gamma = w/n$. This produced the classic picture (see Fig. 6.3 of Peale 1977) in which he showed that tides will tend to drive the satellite to whichever generalized Cassini state is contained within the same separatrix loop (through S_4) as the initial condition. Thus, satellites which would precess around S_1 if there were no tides will be driven to S_1, and similarly for S_2. Peale also found that S_3 is unstable: objects whose spin obliquities are larger than that of the S_4 separatrix (including most retrograde spins) would have their endpoints—neglecting effects due only to the synchronous spin lock—decided by their initial conditions, which would determine which of S_1 or S_2 the trajectory would be drawn to as it "crossed" the S_4 separatrix. Numerical integrations which follow the tidal dissipation of the spin rate are now quite feasible, and we show below that the picture just sketched is largely, but not entirely, correct. The main difficulty is due to the fact that although both S_1 and S_2 are attractive in θ, ϕ space, one of them is usually spin-rate unstable for an axisymmetric satellite.

To understand this, we must study the flow of Eqs. (17). We might hope to analyze these equations by setting $\varepsilon = 0$ and studying the unperturbed system (the regular Cassini equations (10)). However, because $\dot{\omega} = 0$ in the $\varepsilon = 0$ limit, the system is structurally unstable (see Guckenheimer and Holmes 1983) and Eqs. (17) are considered a singular perturbation problem. As a result, none of the features of the unperturbed system (such as equilibria, closed orbits, etc.) that exist for the Cassini state equations (10) can be guaranteed to exist for $\varepsilon \neq 0$. In fact, the small ε terms in the axisymmetric system lead to behavior that is qualitatively different from that of the Cassini equations. First note that the very high obliquity branch of fixed points related to S_3 is removed. This is easily seen since $\dot{\omega} = 0$ in Eqs. (17) requires

$$\omega = \gamma \frac{\cos\theta}{1 - (1/2)\sin^2\theta}, \tag{18}$$

which is impossible for $\theta > \pi/2$, since ω is strictly positive and the right hand side is negative. The S_3 branch is thus rendered non-existent by tides (an excellent example of the structural instability of the problem; the branch is not simply made unstable, it is completely removed by the global bifurcation), and no axisymmetric satellite can ever find spin stability at obliquities larger than 90° (within the approximations of our model). Full equilibrium requires that (18) be satisfied, which is true on a two-dimensional surface in (ω, θ, ϕ) space called the $\dot{\omega}$ null cline (although it is clearly independent of ϕ, ε, and i). The $\dot{\theta}$, $\dot{\phi}$ null cline is almost identical to the locations of the fixed points in the Cassini problem since $\varepsilon \ll 1$. Only if $\omega \sim \varepsilon\gamma/\sin i$ and θ is not small does the new term in the $\dot{\theta}$ equation modify the structure. This actually creates a *second* saddle-node bifurcation, connecting the previously distinct S_2 and S_4 branches, as discussed by Quinn (1995).

The equilibrium points of Eqs. (17) are determined by overlaying the $\dot{\omega}$ null cline onto the $\dot{\theta}$, $\dot{\phi}$ null cline. Figure 5 shows a sequence of these null clines for various values of γ. The $\dot{\theta}$, $\dot{\phi}$ null cline is so weakly dependent on γ that we have chosen to use $\gamma = 0.032$ corresponding to Mimas. Every $\dot{\omega}$ null cline tends to $\omega = 0$ as $\theta \to \pi/2$ and to $\omega = \gamma$ for small θ. For any given value of γ the $\dot{\omega}$ null cline usually intersects the $\dot{\theta}$, $\dot{\phi}$ null cline only once (except in a small range of γ discussed below, where the S_1, S_4 saddle-node bifurcation appears). These intersections determine the approximate location of the real equilibrium points of the axisymmetric system (approximate since the plotted $\dot{\theta}$, $\dot{\phi}$ null cline will depend on i and γ, but this dependence is *very* weak for the small inclinations and gammas of most planetary satellites).

The sign of $\dot{\omega}$ changes as the null cline is crossed. Thus trajectories that exist to the right and above the line $\dot{\omega} = 0$ drift to the left (in this region $\dot{\omega} < 0$) while trajectories to the left and below this line drift to the right ($\dot{\omega} > 0$). We see that for small γ the only null cline intersection occurs along the S_1 branch, and that for large γ the only intersection occurs along the S_2 branch. Almost all planetary satellites (excepting the Moon) are in the former regime.

To illustrate the consequences of these points, we overlay three sample trajectories of the axisymmetric system onto the previous diagram for $\gamma = 0.4$. Figure 6a shows the damping of a satellite that begins at low obliquity, spinning at twice the synchronous rate ($\omega = 2\gamma$). Since this state is to the right of the $\dot{\omega}$ null cline, $\dot{\omega} < 0$ and the spin is reduced on a time scale of $\mathcal{O}(1/\varepsilon)$ (recall that the precession time scale is order unity). Trajectories simultaneously damp (on the same $1/\varepsilon$ time scale) to the nearest $\dot{\theta}$, $\dot{\phi}$ null cline (remember that ϕ is not shown in this projection). In Fig. 6a these considerations simply result in the satellite despinning to the equilibrium point on S_1 while maintaining a low obliquity. In contrast, Fig. 6b illustrates the behavior of the same initial spin vector, excepting that the initial spin rate is now changed to three times synchronous. The satellite is attracted to the S_2 manifold, and drifts along it past the S_1/S_4 saddle-node bifurcation since it is attracted to $\phi = \pi$. The fast oscillation apparent in the figure is the time scale over which the spin vector precesses around the generalized Cassini state. As an approximate view we can think of this as the spin vector following one of the precession trajectories shown in Fig. 2 (the $\omega = 1$ panel being approximately correct at the start of the integration). The satellite is then forced to remain near S_2 until it has despun all the way down to $\omega \simeq \varepsilon\gamma/\sin i$, at which point it encounters the new saddle-node bifurcation at high obliquity, where it "falls off" and tran-

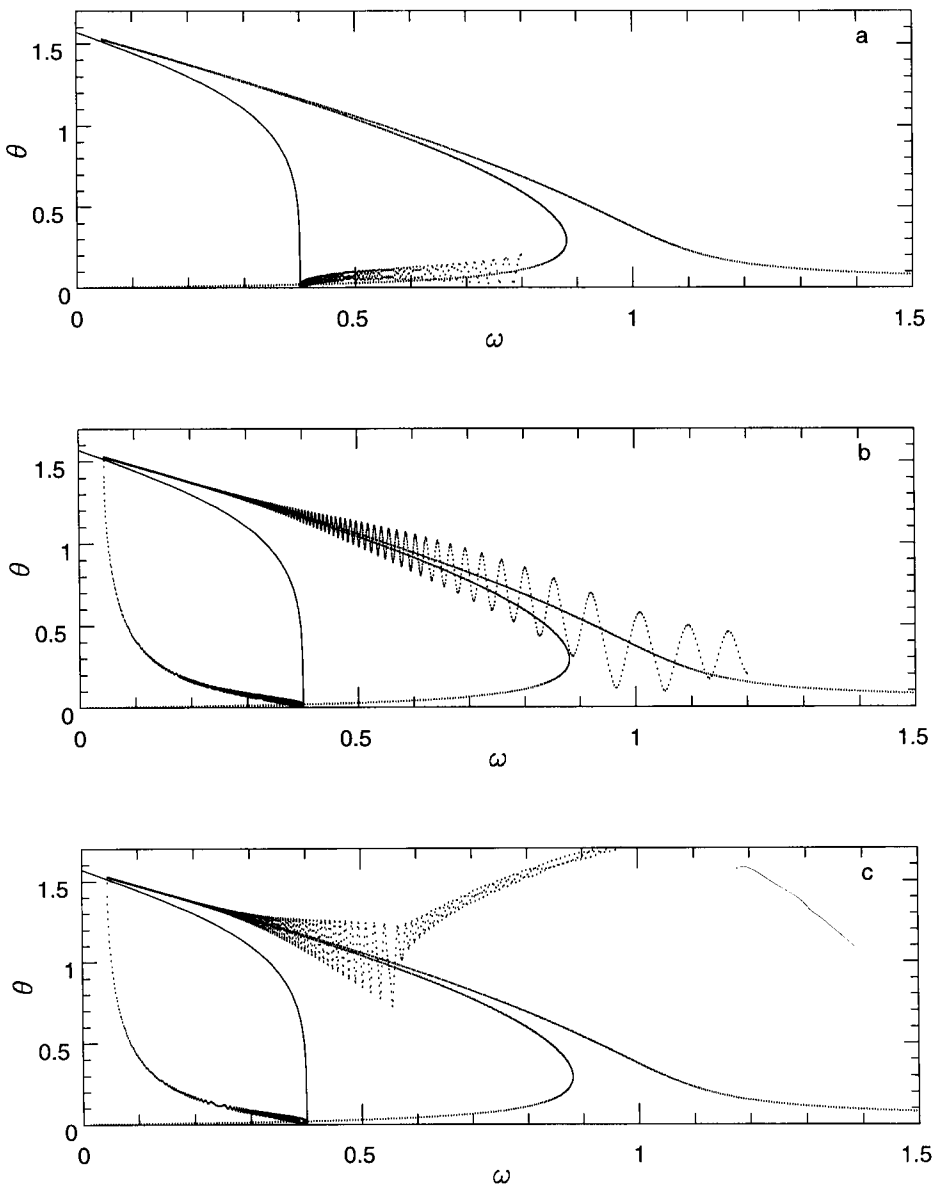

FIG. 6. Trajectories in the axisymmetric system, for the parameter values $\gamma = 0.4$, $i = 1.5°$, and $\varepsilon = 3 \times 10^{-3}$. Three initial conditions are illustrated, with the identical null clines superimposed in each case. All the trajectories eventually reach the only stable equilibrium point given by the intersection of the null clines. (a) An initial condition at twice the synchronous rate ($\omega = 2\gamma = 0.8$) started a low obliquity simply despins (being to the right of the $\dot{\omega}$ null cline) to synchronous rotation. (b) An initial condition started at three times the synchronous rate is attracted to the high obliquity S_2 branch, and proceeds to follow it down to a very low spin rate, before it falls off the S_2 branch at high obliquity (see text). The obliquity is then rapidly reduced and the satellite is spun up (now being to the left of the $\dot{\omega}$ null cline) to the synchronous rate. (c) An initial condition started at three times the synchronous rate but with an obliquity greater than 90° (that is, retrograde spin) is attracted to the high obliquity S_2 branch, and then evolves as in Fig. 6b. It is also possible in this case for the trajectory to pass through the S_2 branch, be attracted to the S_1 branch and proceed directly to the equilibrium point as in Fig. 6a.

sits very rapidly over to the S_1 manifold (this is similar to the phenomena discussed by Holden and Enreux 1993). Notice that in the final regime it is now to the left of the $\dot{\omega}$ null cline and thus its spin rate increases toward synchronous. As a final case, we show in Fig. 6c the evolution of a satellite again started at three times the synchronous rate, but with a retrograde spin ($\theta > \pi/2$). The satellite despins and is captured by the S_2 null cline, along which evolution proceeds as in Fig. 6b; however note that it is also possible to pass through the S_2 null cline, drop down to the S_1 null cline, and go directly to the fixed point (without collecting $200). To aid visualization, we show in

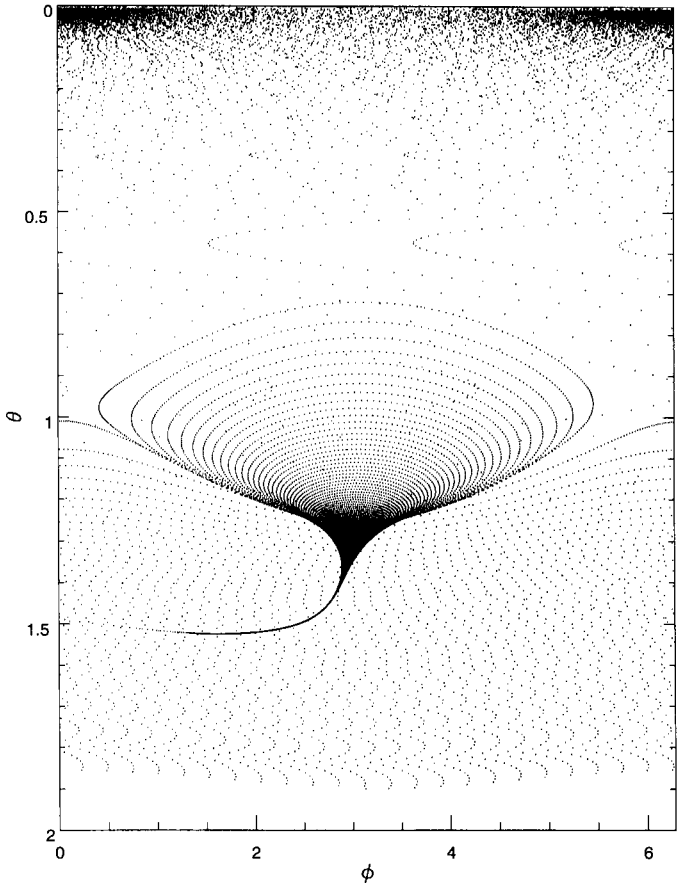

FIG. 7. The trajectory shown in Fig. 6c is here projected onto the ϕ, θ plane (*i.e.*, orthogonal to Fig. 6c). Note that zero obliquity is at the top of the page, so that the low obliquity S_1 state is at the upper corners. The initial condition is in the bottom center ($\theta_0 = 1.9$, $\phi_0 = \pi$). The trajectory evolves upward, is temporarily captured around generalized state S_2, near $\theta = 1$, and damps down to it as its obliquity slowly increases due to the decreasing spin rate. The generalized Cassini state then follows the $\dot{\theta}$, $\dot{\phi}$ null cline and ϕ drifts slowly to lower values until the trajectory passes the S_2/S_4 saddle-node bifurcation. The spin pole then rapidly evolves up to zero obliquity and is captured around S_1, to which it damps.

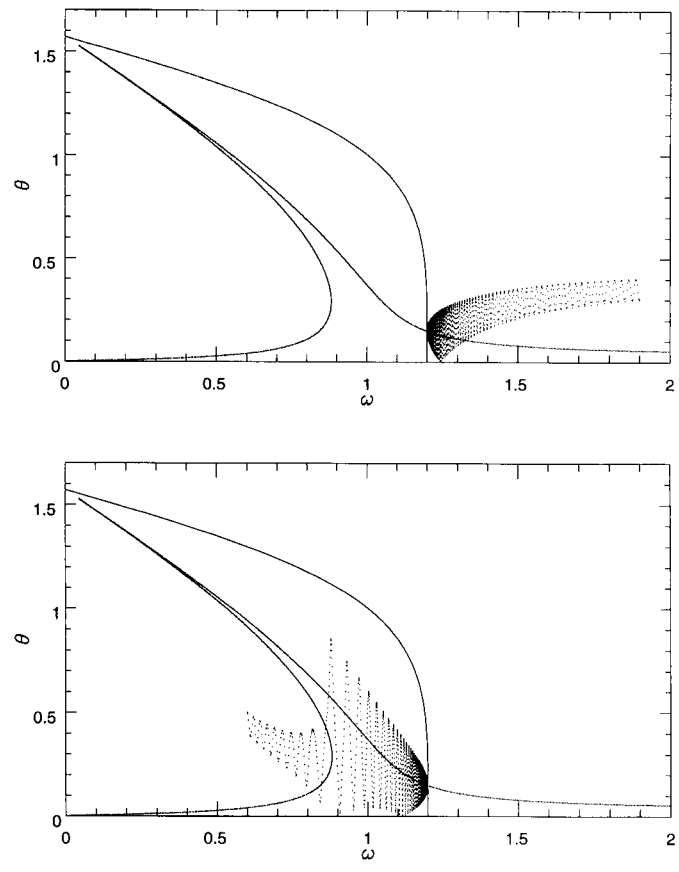

FIG. 8. Two trajectories in the axisymmetric system, for $\gamma = 1.2$, $i = 1.5°$, and $\varepsilon = 3 \times 10^{-3}$. Changing the value of γ has shifted the location of the equilibrium point. The null clines are superimposed in both cases; again the only available end state is given by their intersection. (a) An initial condition above synchronous simply despins to the fixed point. (b) Initial conditions below synchronous are forced to spin up. This particular trajectory exhibits an expected change in precession amplitude as the lower saddle-node bifurcation is passed when S_1 (which it had been precessing around) disappears.

Fig. 7 the Fig. 6c trajectory projected onto the ϕ, θ plane. The initially high obliquity spin vector is captured into libration around S_2, and gradually damps down to the equilibrium point. However, the spin is simultaneously damping and thus the generalized Cassini state about which the libration takes place is gradually moved to higher obliquities, and the trajectory follows this motion. As the spin rate continues to drop, the generalized Cassini state moves away from $\phi = \pi$ (the dark tail in the center of the figure) due to encountering the S_2/S_4 saddle-node bifurcation discussed above, at which point it rapidly evolves up to low obliquities, where S_1 is located.

Similar considerations hold for the large γ case (see Fig. 8). Here initial conditions initially above and below synchronous are driven to the only available equilibrium point, on the S_2 branch, as determined by the intersection of the null clines. In this case the result is more intuitive since the regular Cassini state analysis would claim that only Cassini state S_2 exists, and thus it is logical that this is the only possible endpoint. In contrast, for small γ the classic analysis would indicate that both S_1 and S_2 are possible endpoints, but we have seen that the S_2 branch is in fact spin unstable.

There does, however, exist a narrow range of γ values (approximately from $\gamma = 0.5$ to near $\gamma = \omega_c$; see Fig. 5) for which two stable equilibrium points exist, although this region is probably not occupied by any real satellites. This range is determined by the fact that for θ near $\pi/2$, and writing $\xi = \pi/2 - \theta$, we must have to lowest order $\omega \simeq 2\gamma\xi$ in order to satisfy (18). However, on the $\dot{\theta}$, $\dot{\phi}$ null cline, with $i \simeq 0$ and $\phi \simeq \pi$, we have $\omega \simeq \xi$ near $\theta = \pi/2$. Thus,

even if this null cline reaches almost to $\omega = 0$ (as it will do for $\varepsilon\gamma/\sin i \ll 1$), the two curves will not intersect if $\gamma < 0.5$. The upper limit depends slightly on i, but for small i no second equilibrium point occurs for $\gamma > \omega_c \sim 1$. In fact, only the Moon is known to have $\gamma > 1$, and it is unlikely that any other satellites have $\gamma > 0.1$. (The lunar case is especially interesting since substantial orbital evolution has occurred; see Ward 1975.) Thus, we shall not worry further about this intermediate regime, even though it is the only regime in which there are in fact two stable endpoints, the choice of which does depend on the initial conditions, as was Peale's (1974) original suggestion.

We have also fairly thoroughly explored parameter space for the problem, including large orbital inclinations (up to 30°) and large values of ε (up to almost unity). In these regimes, when γ is of order unity, one finds many interesting dynamical phenomena, including globally stable limit cycles and chaotic attractors. Since these occur for unphysical parameter values we will not present these results here (but see Quinn 1995).

We have seen that the final endpoint in the tidal evolution of a perfectly axisymmetric satellite is determined completely by the value of γ; for $\gamma < 0.5$ only S_1 is accessible, while for $\gamma > \omega_c$ S_2 is the only possibility. Rather surprisingly, we find that for the very small values of γ that are typical for planetary satellites, an initially rapidly spinning object ($\omega > \omega_c$) or one that finds itself near the high obliquity branch, could be driven down to an *extremely* small spin rate of $\omega \sim \varepsilon\gamma/\sin i$ at high obliquity before transiting over to the S_1 equilibrium point at $\omega \simeq \gamma$ and $\theta \sim \gamma \sin i$. This behavior would seem unrealistic since we know that when the satellite crosses $\omega = \gamma$, (*i.e.*, passes through synchronous rotation), any existing triaxiality in the satellite will serve as a moment arm, the torque on which may act to stabilize the synchronous spin rate. This unfortunately complicates our simple picture of tidal evolution and requires a more complete treatment, which we now present.

5. THE COMPLETE EQUATIONS

Planetary satellites are not perfectly axisymmetric. We expect that the torque associated with $B - A$ may have a dramatic effect upon the rotation as a state of near-synchronous spin is reached, and inhibit the sub-synchronous rotation illustrated in Fig. 6b. The dimensionless parameter β (see Eq. (7)) expresses the relative importance of the non-axisymmetric $B - A$ moment compared to the rotation-induced $C - A$ moment. Therefore we now examine the complete set of equations (3)–(6), which include the effects of a permanent non-axial moment of inertia. Recall that $\alpha \gg 1$ (typically $\alpha \simeq 10^4$–10^7). Thus, unless $\omega \simeq \gamma$, ψ_0 (which indicates the position of the long axis of the satellite relative to the planet) varies on an orbital time scale, and circulates at a tremendous rate compared to the other angles (which vary on the precession time scale). Therefore we expect that all the ψ_0 terms will average to zero until the rotation of the body is very close to synchronous. In fact, we expect that the terms involving ψ_0 will be completely unimportant to the qualitative evolution until

$$\omega - \gamma = \mathcal{O}\left(\frac{1}{\alpha}\right) \tag{19}$$

at which point these terms "turn on." Numerical simulations confirm that this is indeed the case. The *average* behavior of the system is perfectly well described by the axisymmetric equations (17) as long as (19) is not satisfied. The axial asymmetry just superimposes a very high frequency oscillation on the ω evolution, with an amplitude proportional to β. We can therefore apply our knowledge of the behavior developed for the axisymmetric case until synchronous rotation is reached.

5.1. *Long-Axis Libration*

In near-synchronous rotation, the $B - A$ torques will completely dominate the system since for all real satellites the β terms are orders of magnitude larger than most of the other terms in the equations (*i.e.*, $\beta \gg \varepsilon$ in the $\dot{\omega}$ equation, and $\beta/\omega \gg 1$ in the $\dot{\theta}$ and $\dot{\phi}$ equations). Because of this, we can gain some insight by ignoring all terms *except* the β terms. Assuming that this results in no net change in θ or ϕ over a complete ψ_0 cycle, we examine just the ω and ψ_0 equations in the limit of small obliquity when there are no tidal terms:

$$\dot{\omega} \simeq -4\beta \sin(2\psi_0)$$
$$\dot{\psi}_0 = \alpha(\omega - \gamma).$$

Combining these into a single equation and switching back to dimensional units yields

$$\psi_0'' + \frac{3}{2}\frac{B - A}{C} n^2 \sin(2\psi_0) = 0. \tag{20}$$

This is the same as Eq. (5) of Goldreich and Peale (1966), used to study the spin–orbit coupling of Mercury, but with the orbital eccentricity set equal to zero. The character of the trajectories of this equation is effectively a rigid rod pendulum equation (doubly periodic since the system is symmetric under $\psi_0 \rightarrow \psi_0 + \pi$). The points ($\psi_0' = 0$, $\psi_0 = \pi/2, 3\pi/2$) are unstable since this effectively interchanges the axes so that $B - A < 0$, in which case (20) has exponentially growing solutions. Should a satellite near $\psi_0 = 0$ (or π) in synchronous lock be struck so as to have its spin rate

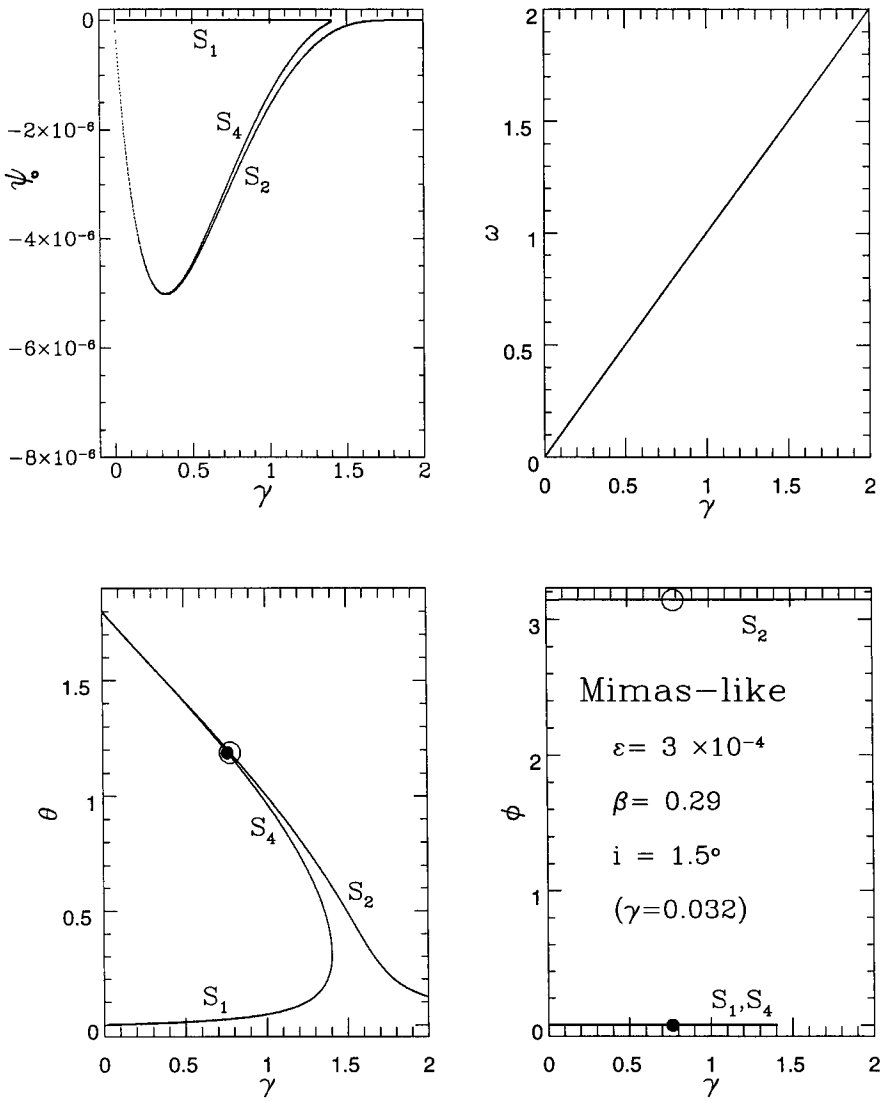

FIG. 9. A bifurcation diagram for the full equations, using the ε, i, and β values appropriate for Mimas. For any value of γ, the location of the fixed points can be located (Mimas has $\gamma = 0.032$). Two unstable branches (ψ near $\pi/2$ and $3\pi/2$) have been omitted. The solid and open dots locate positions on the S_4 and S_2 branches, respectively, where the eigenvalues change sign (the positions of these two dots are close, but not coincident). Note that the S_1 and S_4 branches are superposed on the ϕ plot, but that this plot shows clearly the separation of the S_4 and S_2 branches (compare with the θ plot). See the text for further discussion.

increased by a small amount $\dot{\psi}_0$, the satellite will simply librate about the $\psi_0 = 0$ (or π) fixed point. It is easy to show that as long as $\dot{\psi}_0 < \sqrt{8\alpha\beta}$ (or $\psi_0' < n\sqrt{3(B-A)/C}$ in dimensional units) the satellite will be driven back to synchronous rotation (that is, $\dot{\psi}_0 = 0$) before ψ_0 can complete 1/4 of a revolution (recall that this is ψ_0, not ψ), and the satellite will librate *with constant amplitude* about the fixed point $\psi_0 = 0$, $\omega = \gamma$ on a short time scale (of order the orbital period divided by $\sqrt{(B-A)/C}$).

A simple calculation shows that an impactor of order 10^{-3} of the mass of Mimas, striking its surface obliquely at 20 km/sec, is required to break the synchronous lock. In fact, this would likely shatter Mimas. Close satellites, once they have deformed to a hydrostatic shape, are unlikely to have ever been knocked out of their synchronous locks. However, more distant satellites require a smaller impact since the necessary additional spin rate scales as $n = a^{-3/2}$. Thus Iapetus, for example, could be knocked out of synchronous rotation and damped again, perhaps interchanging the leading and trailing hemispheres. Lissauer (1985) discusses these issues.

Even if not knocked out of its synchronous lock, a disturbed satellite will librate around the fixed point. The tidal torque will then damp out this libration, on

a time scale of order $1/\varepsilon$. To see this, include the tidal term in the spin evolution equation; if θ is librating near zero (*i.e.*, around S_1), then averaged over such a libration we have

$$\dot{\omega} \simeq -\varepsilon(\omega - \gamma) - 4\beta \sin 2\psi_0 \tag{21}$$

$$\dot{\psi} = \alpha(\omega - \gamma). \tag{22}$$

Setting $s \equiv \omega - \gamma$ and linearizing around the fixed point ($s = 0$, $\psi_0 = 0$) gives eigenvalues (to lowest order in ε) of

$$\lambda \simeq -\frac{1}{2}\varepsilon \pm \sqrt{-8\alpha\beta}. \tag{23}$$

The negative real part gives a damping time scale for the libration amplitude of $2/\varepsilon$. Numerical simulations of the full set of equations for low obliquity confirm that this result holds for the full system. For Mimas, this libration damping time scale is approximately 1000 years.

A similar analysis for a system librating around a high obliquity fixed point ($\theta \simeq \pi/2$) yields eigenvalues with real parts of $-\varepsilon/4$, and so it would seem that we should again damp to the equilibrium point, albeit at a slightly slower rate. In fact, we show below that for the high obliquity limit the approximations made in truncating the full system to (21)–(22) are too severe.

5.2. *Bifurcation Diagram*

To learn about the global structure of the full four-dimensional equations, we examine a bifurcation diagram (Fig. 9). Since ε is very small, it has little impact upon the location of the fixed points. Both i and β vary over small ranges, so we use γ (which varies by orders of magnitude) as our tunable parameter. We see that the $\dot{\psi}_0$ equation demands $\omega = \gamma$. To determine the other variables at an equilibrium point, we first solve the $\dot{\omega} = 0$ equation for ψ_0 to give

$$\sin(2\psi_0) = -\frac{\varepsilon\gamma}{2\beta}\left(\frac{1 - \cos\theta}{1 + \cos\theta}\right)^2. \tag{24}$$

We use this to eliminate $\sin(2\psi_0)$ in the $\dot{\theta}$ equation and write

$$\sin\phi = \frac{\varepsilon \sin\theta}{2 \sin i}\frac{3 - \cos\theta}{(1 + \cos\theta)}. \tag{25}$$

Substitution of these results in the $\dot{\phi}$ equation leads to a transcendental equation for the values of θ at which equilibrium points exist,

$$\begin{aligned} 0 = f(\theta) = \pm\sqrt{1 - \sin^2\phi}\,\sin i\frac{\cos\theta}{\sin\theta} + \cos i \\ -\frac{1}{\gamma}\cos\theta \mp \frac{\beta}{\gamma}(1 + \cos\theta)\sqrt{1 - \sin^2(2\psi_0)}, \end{aligned} \tag{26}$$

where the signs on some of the terms depend on which branch of the solutions we pick for the cosines derived from (24) and (25). Two of the ψ_0 branches (ψ_0 near $\pi/2$, $3\pi/2$) are always unstable (the long axis being perpendicular to the direction to the planet), so we will only consider the branches near 0 or π; thus we choose the negative sign on the β/γ term in (26). We can solve for the zeroes of the function $f(\theta)$ to find the equilibrium value of θ and then use (24) and (25) to determine the location of the equilibrium points. Clearly for small ε we expect both ψ_0 and ϕ to be close to 0 or π, and (26) reduces essentially to the Cassini state expression (16) for $\omega = \gamma$. Figure 9 shows a bifurcation diagram for the parameter values appropriate to a Mimas-like object (γ is tunable, so the diagram locates the equilibrium points for Mimas only for $\gamma = 0.032$). A similar diagram for a Moon-like object is shown as Fig. 10. In these diagrams, the small deviations of ψ_0 and ϕ from the values 0 or π represent the balance between the solid body and residual tidal torques at synchronous rotation. Note that the latter is non-zero for $\theta \neq 0$ (see Eq. (48) in Appendix A).

Figures 9 and 10 are qualitatively similar to that for the Cassini problem (cf. Fig. 4), but there are some important differences. The tunable parameter is γ, not ω (ω is of course forced to be γ at the equilibrium points). The S_1, S_4 saddle-node bifurcation has moved to a larger value of γ since the Cassini state positions are influenced by the β term (see Eq. (16)). The S_1 branch behaves as before, and the S_2 branch still goes to small obliquities ($\theta_2 \to i$) for large spin rates. On the S_1 branch, at synchronous rotation for $\gamma \ll 1$, equilibrium in (15) implies that $\sin\theta_1 \simeq \gamma \sin i/(1 + 2\beta)$. An important change is that for large obliquities the S_2 and S_4 branches are no longer asymptotic to $\theta = \pi/2$. This is because the $\dot{\phi}$ equation has been radically modified at small spin rates. These high obliquity branches must approximately satisfy

$$1 - \frac{1}{\gamma}[\cos\theta + (1 + \cos\theta)\beta] \simeq 0,$$

since i and ψ_0 are small, and cot θ does not diverge. The first term ($\cos i$ to lowest order) is simply the orbit-precession induced change in ϕ. For most satellites, $\gamma \ll 1$, and so the second term must be made small by the obliquity contributions. When β was zero, this was simply done by having $\theta \to \pi/2$ and thus $\cos\theta \to 0$, representing decreasing the averaged torque on the oblateness of the satellite by bringing the rotation pole close to the orbit plane. With a perma-

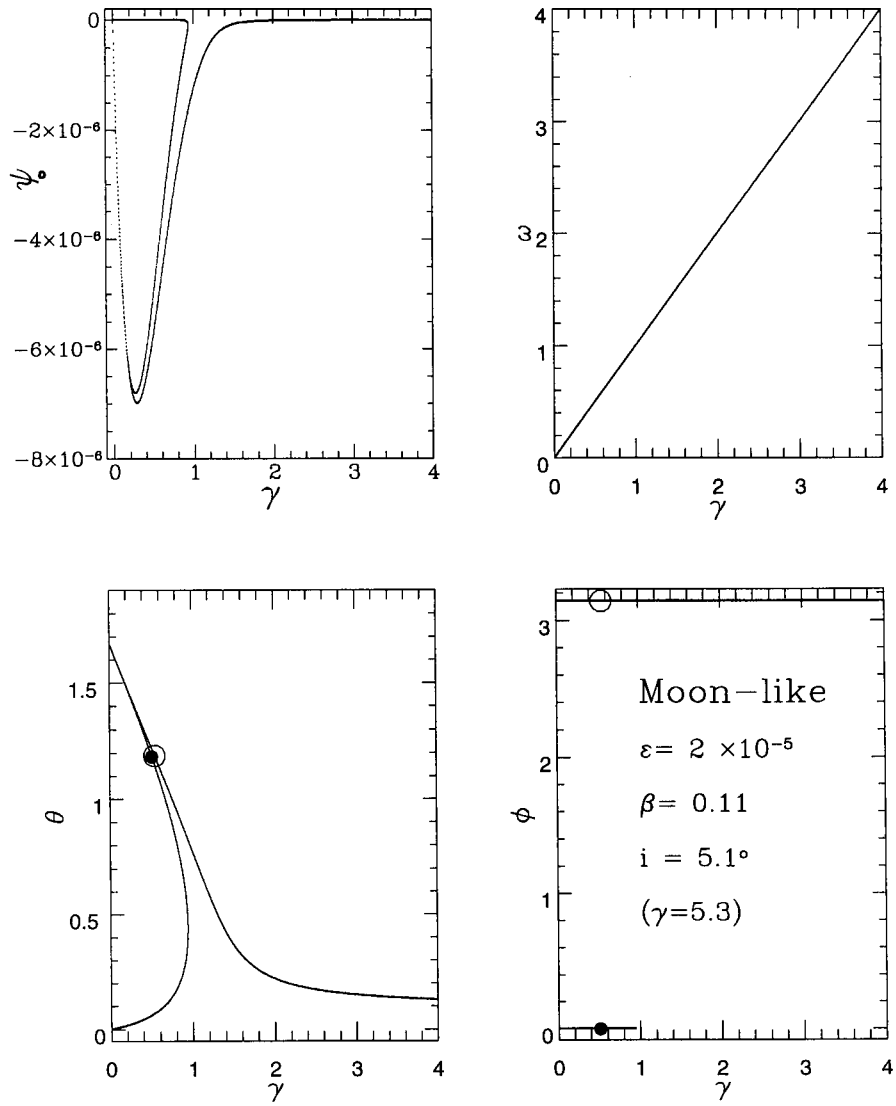

FIG. 10. A bifurcation diagram for lunar parameter values. See the caption to Fig. 9.

nent non-axial deformation, this no longer eliminates the averaged torque since the nonaxial torque remains. In fact, the two solid body torques must be balanced against each other, which implies an obliquity greater than 90°. The requirement on θ is

$$\cos\theta_2 \simeq \frac{\gamma-\beta}{1+\beta}. \tag{27}$$

For small γ, which is typical, this requires $\cos\theta_2 < 0$. For $\gamma > \beta$ this condition is not relevant because the obliquities become small and the first term of the $\dot{\phi}$ equation cannot be ignored.

The stability of the fixed points was determined by a linear analysis and examination of the eigenvalues at each point. The S_1 branch has four complex eigenvalues with negative real parts and is thus always stable in the full problem. The S_4 branch always has two of its four eigenvalues strictly real, one positive and the other negative. The other two eigenvalues on the S_4 branch change sign below a certain value of γ (shown by the solid dot in Figs. 9 and 10). These two eigenvalues are complex, with positive real parts for γ smaller than this value, and with negative real parts above it (until the S_4 branch ceases to exist at the saddle-node bifurcation). Thus S_4 is still unstable with the inclusion of the $B - A$ terms, and exponentially so since the positive real root, corresponding to the saddle structure, is large. The S_2 branch shows a similar behavior, with the real parts of two of its four complex eigenvalues changing sign. Above a particular value of γ (shown by the open

circle in the figures) it has four complex eigenvalues with negative real parts (as does S_1) and is therefore stable, but below this value the complex eigenvalues have two negative and two positive real parts, and the fixed point *is thus unstable*. The positive real parts are both small, and the instability occurs only on the tidal time scale. This is an extremely important result since most planetary satellites have $\gamma \ll 1$ and thus, if they were ever at high obliquity, would lie in this regime. The location of the change in stability of S_2 and S_4 is not a strong function of β. Decreasing β by an order of magnitude from the values shown in Fig. 14 only lowers the stability changeover points by a factor of 2 in γ. Thus, a very small primordial value of β will not result in the upper branch of fixed points being freed from their instability. In summary, S_1 is stable, and S_4 unstable, for all values of γ (for which they exist). S_2 is stable only for values of γ *greater* than the value indicated by the open circle (at order unity).

We present in Appendix B a calculation showing that there is a critical value of the obliquity $\theta_{cr} \simeq 68° \simeq 1.18$ radians above which all fixed points in the bifurcation diagram are unstable. Observe in Figs. 9 and 10 that the stability changeover points all occur for this value of the θ, regardless of the value of γ at which the branches first satisfy this condition. The lack of stability of this high obliquity branch is best discussed in conjunction with the results of our numerical studies.

5.3. *Numerical Results*

Numerically, we are facing the daunting computational task of following the spin behavior of the satellite (on a time scale of $1/\alpha$), but for tidal evolution time scales, $\mathcal{O}(1/\varepsilon)$. Thus the numerical "dynamic range" required is $\mathcal{O}(\alpha/\varepsilon) \sim 10^6$–$10^{13}$. Only recently has computer hardware advanced to the point where the lower end of this range is feasible. Since Mimas has $\alpha/\varepsilon \simeq 3 \times 10^7$, we will use it to illustrate our results, but firmly believe that our results are insensitive to the changes in these parameters. In fact, for the purposes of the integrations in regards to both computational speed and ease of viewing the evolution in the figures, we have increased ε by a factor of 10. We have confirmed that the resulting evolutions are simply sped up by the same factor; the final states and all the qualitative features are identical to the more exact integration.

The most common case of interest would be that of a satellite with $\gamma \ll 1$ having its libration damped to S_1. This is illustrated in Fig. 11, for the case of Mimas starting at twice synchronous. The time step in the integrator (we used a simple fourth order Runge–Kutta algorithm) is smaller than the spin period in the rotating frame (*i.e.*, $d\tau \ll 1/\alpha$) in order to correctly average out the effects of the axial asymmetry. For Mimas this requires a time step 10^4 times smaller than used before in the calculations of Figs. 6–8. As discussed above, for $\omega > \gamma$ the average behavior of $\omega(\tau)$ is the same as in the axisymmetric system, but with a high frequency oscillation superimposed. Only when $\omega \simeq \gamma = 0.032$ is reached do the β terms in the equations turn on, at which point the long axis of the satellite is captured into libration. At this point the pendulum equation (20) is the correct approximate view of the phase space, and the libration is gradually damped out by the tidal terms, on a time scale of $\mathcal{O}(2/\varepsilon)$, as predicted by (23). In Fig. 11 the continued circulation of ϕ is an artifact of the coordinate system, since the spin axis is very close to the pole.

Synchronous locking to S_2 in the lunar case is very similar to the Mimas case, and will not be illustrated. Note that the instability of the S_2 branch discussed above is not relevant to the lunar case since the final obliquity of $\simeq 6.7°$ is smaller than $\theta_{cr} \simeq 68°$. We also will not illustrate the evolutions of satellites that begin at high obliquity and evolve directly to S_1. This reasonably common behavior (which could occur in Fig. 6c if the trajectory had passed through the S_2 branch and fallen directly down to S_1) depends on the initial conditions, but does not bear directly on our question of the non-occupancy of S_2.

Our final topic is the behavior of satellites that find themselves near the high obliquity branch of fixed points (the low γ, high θ region in Fig. 9). In the previous section we observed that a perfectly axisymmetric satellite which was attracted to the upper branch would be forced to spin down to extremely small spin rates ($\omega \simeq \varepsilon\gamma/\sin i$; see Fig. 6b) before eventually crossing over to the S_1 state. This behavior seems unlikely, since as synchronous rotation is passed axial asymmetries would be expected to lock the spin rate, trapping the satellite in S_2. However, the bifurcation diagram (Fig. 9) shows that fixed points along the upper branch are unstable above θ_{cr}.

In fact, we find that for the realistic parameter values of Table II, satellites are never drawn even close to the high obliquity fixed point. Trajectories that are initially attracted to the high obliquity branch (and thus are in some sense precessing around S_2 in a narrow range of θ near $\pi/2$ as in the $\omega = 0.1$ panel of Fig. 2) do not approach the full (four-dimensional) equilibrium state. What happens instead is illustrated in Fig. 12, in which a trajectory initially attracted to the S_2 branch is displayed, picking up the evolution at twice synchronous. The time scale for damping the precession amplitude around the fixed point is comparable to the time scale for damping the spin rate to synchronous (*cf.* Fig. 6b), so the spin vector still has some reasonably large amplitude in θ around the generalized Cassini state. (The precession around the generalized Cassini state is visible as the dark ellipse near $\theta = \pi/2$ in the lower left panel of Fig. 12.) Then, as ω approaches γ, the synchronous lock dramatically alters the behavior. The satellite "rolls up" to S_1, with a short period of sub-synchro-

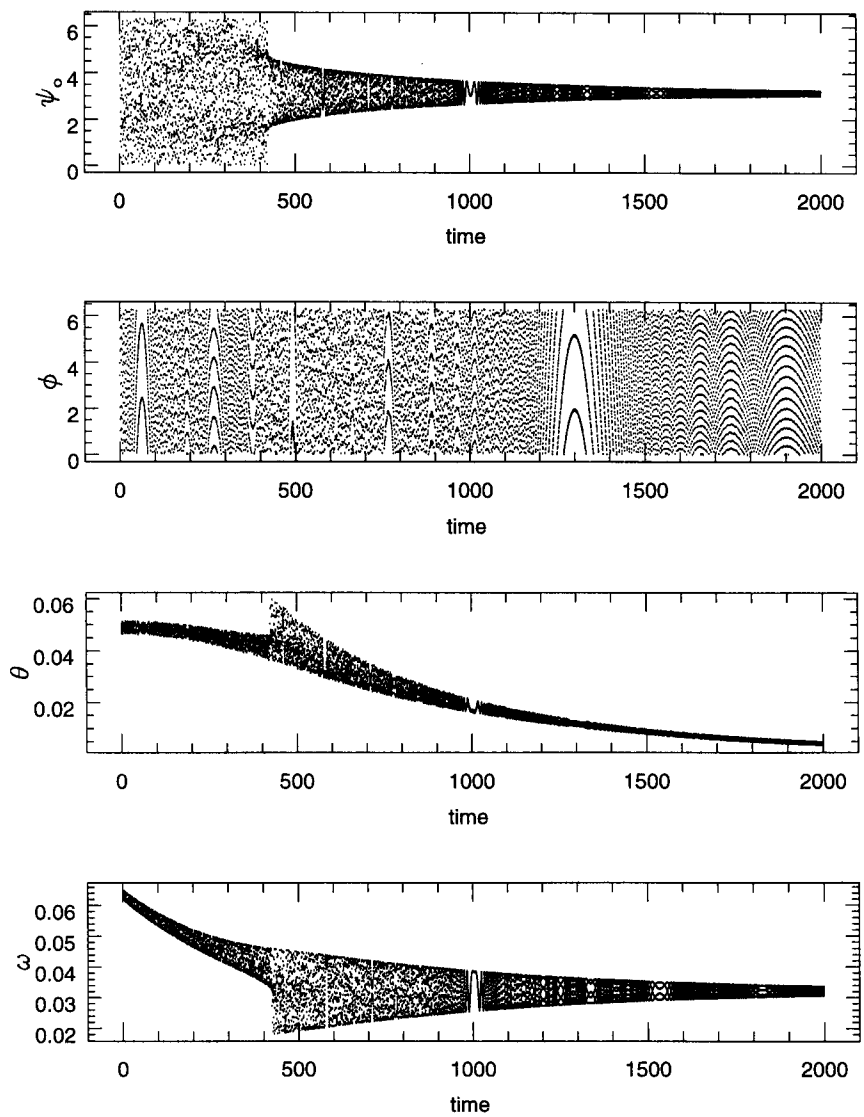

FIG. 11. An illustration of synchronous capture. Mimas is started at twice the synchronous spin rate, and despins until ψ_0 is captured into libration at $\tau \simeq 430$ (corresponding to 685 years of real time). The structure visible in the plots is due to beating between the various precessions and the output sampling rate. Note that after the lock ω oscillates above and below synchronous and that the amplitude of the obliquity libration increases.

nous behavior (which is not unexpected for a high obliquity satellite being acted upon by tides; see Section 4.1). This basic pattern of behavior, with minor modifications, is followed by all high-obliquity satellites that we have integrated which spin down along the upper branch. Note that during the sub-synchronous phase, the mean spin rate continues to drop until the $\dot{\omega}$ null cline is crossed, so the axisymmetric system is, even at this stage, an approximate guide.

However, during the period after ω drops below 0.04 in Fig. 12, the β terms are never really negligible. This is illustrated by the $\omega(t)$ plot, in which the amplitude of the fast oscillation is evidence of the contributions of these terms. One possible interpretation of the post-S_2 behavior, as originally suggested by Peale (1974), is that we may view the problem in terms of the Cassini state precession trajectories of Fig. 2. Examining the $\omega = 0.1$ panel, we view the trajectory just before the synchronous lock as precessing around S_2, inside the "critical parabola" that is really the separatrix through S_4. However, as Eqs. (12) and (16) show, the position of the Cassini state will suddenly shift to higher obliquity when the β terms cease to average out. This results in the critical parabola suddenly "jumping" down the sphere (this is illustrated in Jankowski *et al.* 1989). If the spin vector is left above the new critical trajectory then the

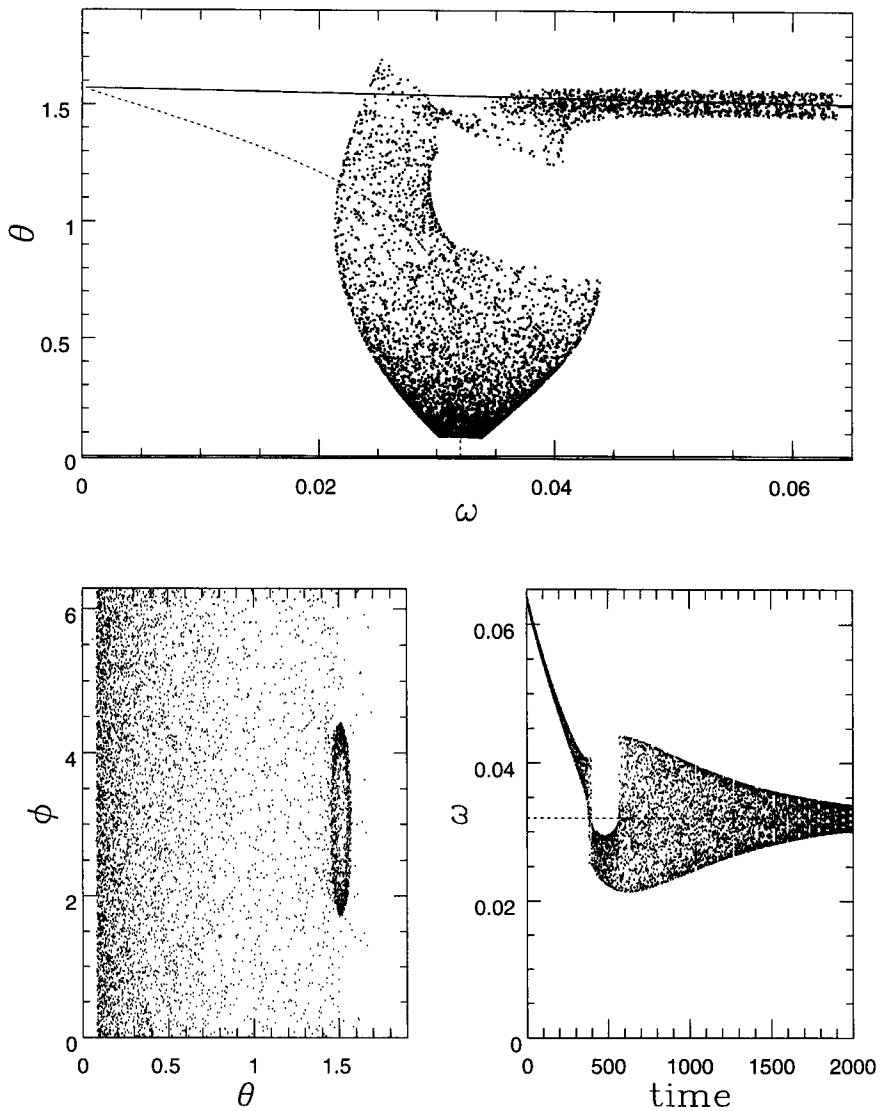

FIG. 12. Spin damping of an initially rapidly rotating (5× synchronous) Mimas. A factor of 10 increase in ε has been used to facilitate viewing. The spin axis is initially librating around the high obliquity branch ($\theta \simeq \pi/2$, $\phi \simeq \pi$) and follows it down to low spin rates. However, as synchronous rotation is approached ($\omega \simeq \gamma = 0.032$) the satellite rolls up to the low obliquity S_1 state. The null clines for the axisymmetric system are shown in the top panel for reference, and the synchronous spin rate is shown as the dashed line in the bottom right panel.

tides would proceed to damp the obliquity to S_1. In fact, this interpretation seems to explain Fig. 12 quite well if we assume that the β terms are always acting below $\omega \simeq 0.45$.

The situation is somewhat more complicated than this if we wish to explain why *no* primordial satellites were trapped in S_2, because the amount that the critical parabola shifts depends on β. If primordial satellites had smaller values of β than those we assume here, or large orbital inclinations (e.g., Triton–see Jankowski *et al.* 1989), it is not clear that the critical parabola jump would always be sufficient to remove the satellite from S_2. However, we saw before that in fact the high obliquity fixed point of the full equations is unstable for $\theta > \theta_{cr}$. Even if we *exquisitely* tune the variables so that the satellite is started very near this equilibrium point, behavior like that shown in Fig. 13 results. The linear stability of the θ and ϕ equations is apparent; more importantly, this figure shows that the two eigenvalues with positive real parts produce an unstable growth in the libration amplitude of the long axis. The ultimate consequences are shown in Fig. 14; the libration grows until the long axis breaks into circulation and the satellite then evolves to lower ω along the S_2 branch until it "falls off" and is damped to the low obliquity (S_1) state. This figure is very interesting because it is illustrative of all of the restricted problems discussed in this paper. In

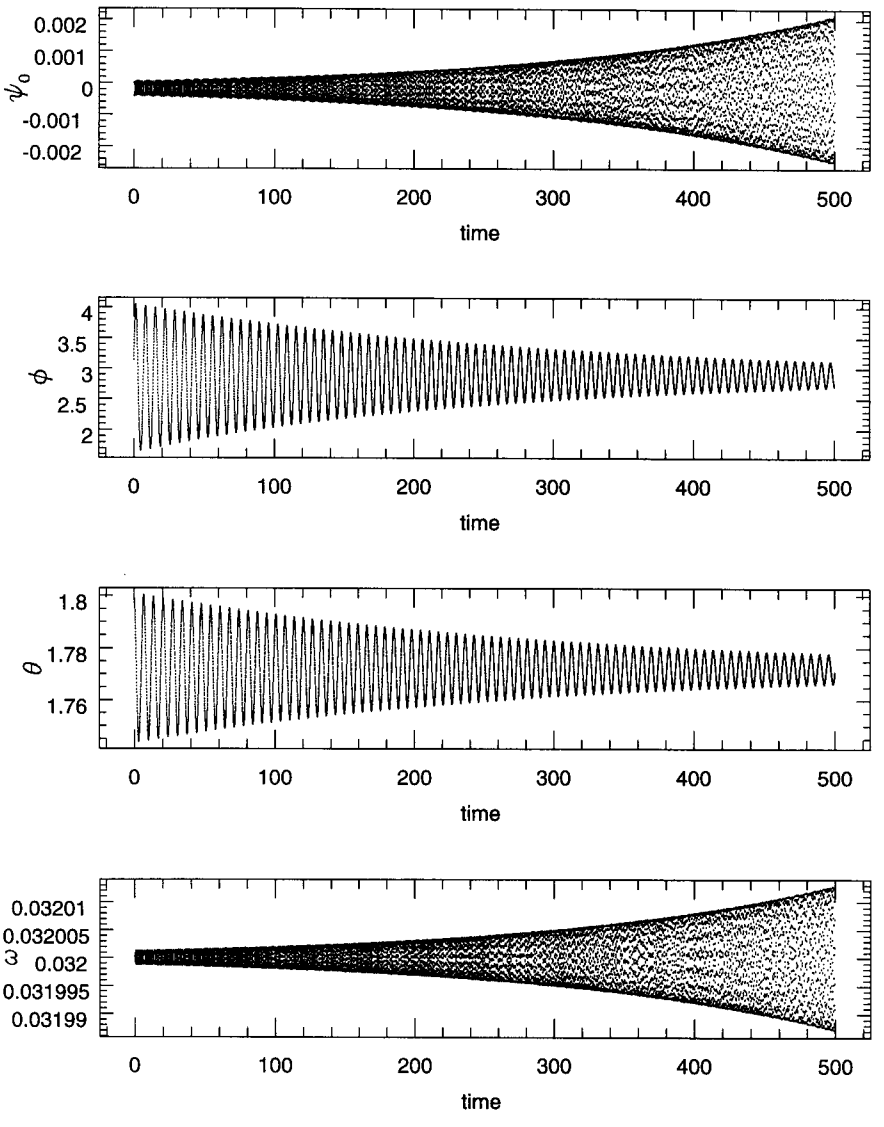

FIG. 13. Instability of S_2 in the full equations. An object started with Mimas-like parameters near the high obliquity fixed point is driven toward it in the θ and ϕ variables, but ψ_0 and the spin rate ω exhibit an instability.

the initial and final states where ψ_0 is librating, the pendulum-like equation (20) is the best approximation. The satellite breaks free at $t \simeq 2250$ and once ψ_0 begins to circulate the axisymmetric system is the appropriate view of the system (as evidenced by the monotonic drop in ω). In fact, over short time scales during this period over which the spin is roughly constant, the generalized Cassini state picture is valid, with the spin pole precessing around S_2 on a skinny ellipse (since the θ amplitude is small while the ϕ amplitude is large). This lasts until $t \simeq 3700$ when the trajectory encounters the axisymmetric system's S_2/S_4 saddle-node bifurcation at $\omega \simeq \varepsilon\gamma/\sin i \sim 0.003$, whereupon the obliquity drops dramatically (as in Fig. 6b). The axisymmetric regime ends at $t \simeq 4100$ when the long axis is again captured into libration, which is then damped as the system approaches the only stable equilibrium point of the full set of equations, at S_1.

Thus, even if the satellite remained inside the critical parabola after the synchronous spin lock, the tidal instability of the fixed point prevents the satellite from damping to synchronous rotation at S_2. This also holds for any satellites which, for any reason, find themselves near the upper obliquity branch close to synchronous rotation. We believe that it is ultimately for this reason that satellites with low values of γ cannot be found in Cassini state S_2.

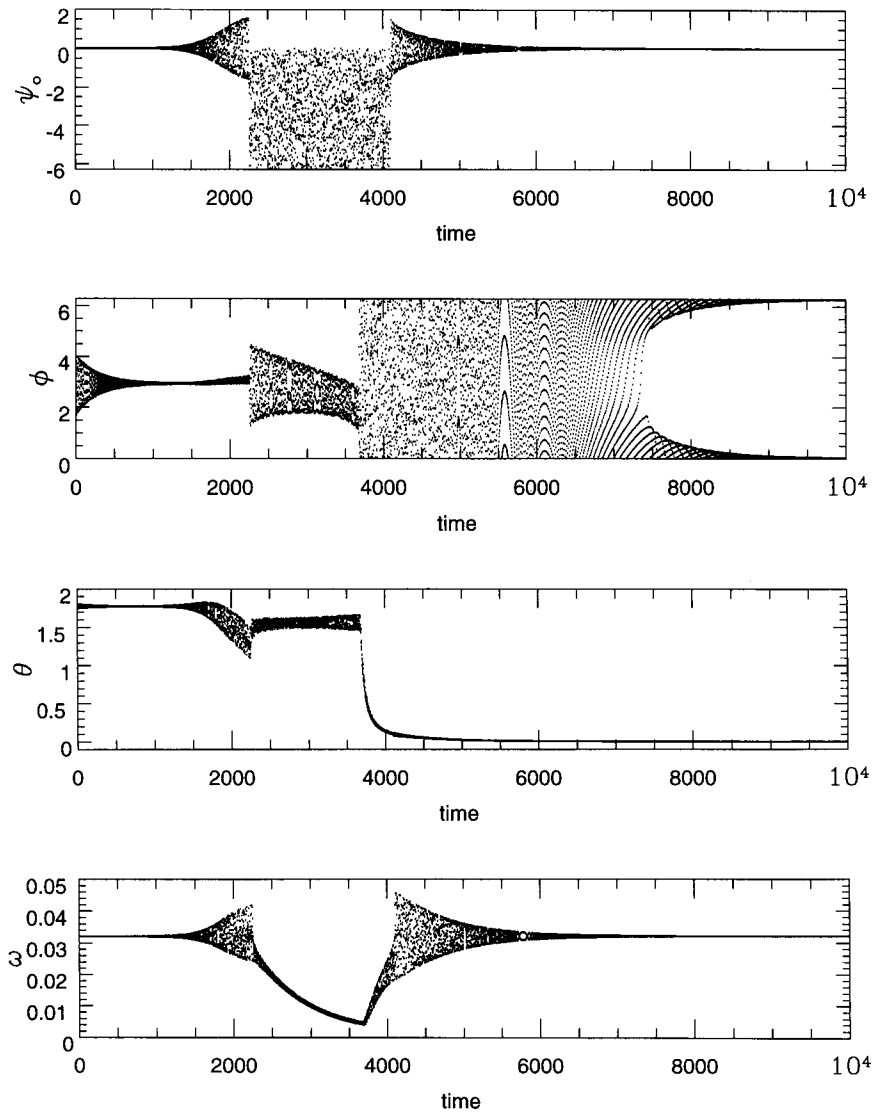

FIG. 14. A continuation of the simulation of Fig. 13. The libration amplitude grows until ψ_0 begins to circulate. At this point the precession around S_2 (in θ, ϕ) slowly drifts and the spin rate drops until the S_1/S_4 saddle-node bifurcation of the axisymmetric problem is crossed, at which point the obliquity θ is rapidly damped to near zero. The satellite is then captured by and damped to S_1 at synchronous rotation.

6. DISCUSSION AND CONCLUSIONS

The conclusion that the S_2 state is unstable for small γ should not be sensitive to our approximations. Although it is true that the wobble decay times may not be negligible compared to the despinning times for some satellites, the wobble will eventually damp out and should the satellite be near S_2 the instability illustrated in Fig. 13 will result in its removal from that state. Perhaps more interesting is the importance of the possibility of chaotic tumbling to our results. Wisdom (1987) showed that irregular satellites on eccentric orbits would begin to tumble as their long axes attempted to switch from circulation to libration. Through a limited number of numerical simulations of the full Euler equations of motion, including the solid body although not tidal torques, and abandoning the principal-axis assumption, we find that the most irregular satellites (e.g., Phobos) do indeed tumble during the passage into libration, even when their orbits are circular. More regular objects (e.g., Mimas) do not, and a comparison of the Euler integration with Eqs. (3)–(6) shows an excellent match at low obliquity. At high obliquities, using current moment differences like those in Table 2, we find that the satellites are unstable to tumbling for spin rates as high as twice synchronous. Thus details of trajectories computed from the averaged equations for irregular satellites at high obliq-

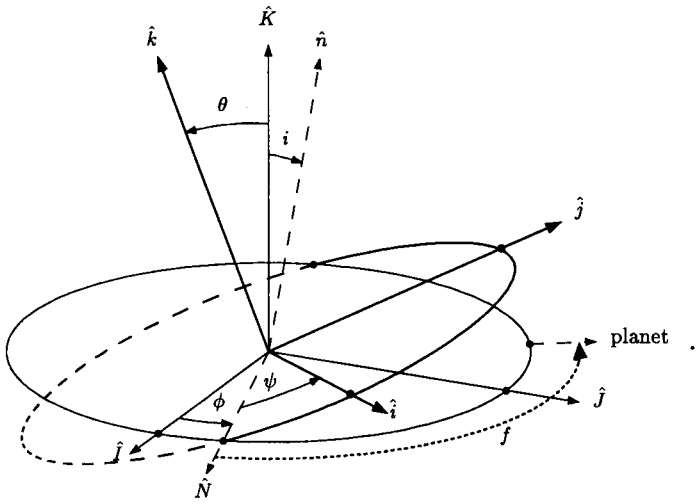

FIG. 15. Coordinate system for the problem. Here all of the angles shown in Fig. 1 have been transferred to a single origin. The **IJ** plane is the orbit plane, while the **ij** plane is the equatorial plane of the satellite. The invariable plane normal **n** is in the **JK** plane. The ascending node **N** is in the direction $\mathbf{K} \times \mathbf{k}$, and is where the anomaly f of the planet is measured from. The θ, ϕ, ψ variables are the usual Euler angles (but note that $\psi_0 = \psi - f$, not ψ, appears in the averaged equations of motion).

uity (e.g., Fig. 12) are undoubtedly incorrect. Only *very* close to S_2 ($\omega < 1.1\ \gamma$, θ within 0.1 radians of θ_2) does the tumbling motion cease in the Euler integration (which neglects tidal effects).

Beletskii (1972) showed that near-synchronous satellites that are in principal axis rotation about the short axis, with their long axis pointed at the planet, are prone to wobble instabilities if $58°15' < \theta < 97°15'$. His model neglects tidal effects; the physics of this instability is thus completely different from the tidal instability of the previous section, which persists for all $\theta > 68°$. Moreover, from (27), the location of S_2 for satellites with $\beta \simeq 0.3$ and $\gamma \ll 1$ is $\theta_2 \simeq 103°$, so S_2 would be at higher obliquity than the wobble instability regime for most natural satellites.

Our intent has been to find a reason why no satellites can be in Cassini state 2. Although several possibilities have been advanced in the literature (collisions knocking satellites out of S_2, the spin lock shifting the critical parabola, or wobble instabilities), none of these suggestions really firmly establishes why some satellites could not have avoided these processes. The tidal instability that we present is *unavoidable*, and no satellite can exist in principal axis rotation near S_2 for large obliquity.

In conclusion, we have derived orbit-averaged equations for the evolution of the spin vector, including non-axisymmetric terms corresponding to the resonant argument (ψ_0) at synchronous rotation. In doing this, we have adopted the principal-axis assumption that most previous authors have invoked; this approximation is probably quite reasonable for satellites that begin at high rotation rates (since their wobble-decay time will be short compared to the despinning time) and for those that remain at low obliquity. We have used a simple, physically-motivated tidal model with $Q \sim 1/(\text{frequency})$. The non-dimensionalization of the equations then reveals the fundamental parameters that govern the behavior. The axisymmetric system of equations discussed in Section 4 is fruitfully viewed as a superposition of the regular Cassini problem (Fig. 2) and a slow drift in ω due to the tidal effects. The only equilibrium point for the axisymmetric system is S_1 for $\gamma \simeq \mu/\hat{\Omega} \lesssim 0.5$, and S_2 for $\gamma \gtrsim \omega_c$ (Fig. 5). Two endpoints (i.e., S_1 or S_2) are possible only in the narrow range $0.5 < \gamma < \omega_c$, where real satellites are unlikely to be found. Figure 6 illustrates some typical evolutionary trajectories.

The full set of equations requires synchronous rotation ($\omega = \gamma$) for equilibrium, and near this rotation rate the libration of the long axis is the dominant phenomenon since the torques produced on the $B - A$ moment are very large. Linear stability analysis shows that tidal effects cause librations to be damped around S_1 whenever it exists; however, S_2 is unstable in the full problem when it is located at high obliquity (*i.e.*, when $\theta_2 > \theta_{cr} \simeq 68°$). Numerical integrations confirm this expected capture into synchronous rotation at S_1, and the long-term instability of S_2 (see Figs. 12–14). Integrations of initial conditions that are found near S_2 show that damping to this state does not occur for $\gamma \ll 1$ due to the tidal instability, and thus capture into S_1 is *inevitable*. Since it seems that all tidally despun planetary satellites except the Moon satisfy $\gamma \ll 1$, we have a firm explanation for the lack of tidally evolved satellites found in high obliquity spin states.

7. APPENDIX A

A satellite's rotational motion may be described using two coordinate systems defined by the sets of orthogonal unit vectors {**ijk**} and {**IJK**} (see Fig. 15). The **IJK** system is fixed with respect to the precessing orbit, with **K** defined by the orbit normal. **I** is defined by the ascending node of the orbit on the invariable plane, while **J** completes a right-handed triad. The **IJK** system regresses about the normal to the invariable plane, **n**, with constant angular velocity

$$-\mu\mathbf{n} = -\mu(\sin i\mathbf{J} + \cos i\mathbf{K}), \tag{28}$$

where i is the (constant) orbital inclination relative to the invariable plane.

The second set of unit vectors {**ijk**} is body-fixed and aligned with the principal axes of its inertia ellipsoid. Its orientation with respect to the orbital axes is specified by the Euler angles ϕ, θ, and ψ, as shown in Fig. 15. The spin axis is assumed to coincide with the axis of maximum inertia, **k**, so that the rotational angular velocity $\mathbf{w} = w\mathbf{k}$

and the satellite's obliquity $\theta = \cos^{-1}(\mathbf{k} \cdot \mathbf{K})$. Note that the obliquity is measured with respect to the instantaneous orbit normal **K**. The ascending node of the satellite's equator (i.e., **ij**) plane on its orbital (**IJ**) plane is defined by the unit vector $\mathbf{N} = \mathbf{K} \times \mathbf{k}/\sin\theta$. In the **IJK** system

$$\mathbf{k} = \sin\theta\sin\phi\mathbf{I} - \sin\theta\cos\phi\mathbf{J} + \cos\theta\mathbf{K} \tag{29}$$

and

$$\mathbf{N} = \cos\phi\,\mathbf{I} + \sin\phi\,\mathbf{J}. \tag{30}$$

The equations of motion in the precessing **IJK** frame are

$$C[w'\mathbf{k} + w\mathbf{k}' - w\mu(\mathbf{n} \times \mathbf{k})] = \mathbf{\Gamma}, \tag{31}$$

where $\mathbf{\Gamma}$ is the external torque exerted on the satellite and primes denote differentiation with respect to time. We may separate $\mathbf{\Gamma}$ into a component $\mathbf{\Gamma}_1$ due to the torque exerted by the planet on the satellite's non-spherical figure, and the tidal torque exerted by the planet $\mathbf{\Gamma}_2$. Before deriving explicit expressions for these torques, we first use (31) to derive the equations governing the variations of w, θ, and ϕ separately. This is done most expeditiously by forming scalar products of the equation of motion with the unit vectors **k**, **K**, and **N** in turn (cf. Goldreich and Peale 1968):

$$Cw' = \mathbf{k} \cdot \mathbf{\Gamma}, \tag{32}$$

$$C[w'\cos\theta - w\theta'\sin\theta + w\mu\sin i\sin\theta\sin\phi] = \mathbf{K} \cdot \mathbf{\Gamma}, \tag{33}$$

and

$$C[w\phi'\sin\theta - w\mu(\sin i\cos\theta\cos\phi + \cos i\sin\theta)] = \mathbf{N} \cdot \mathbf{\Gamma}. \tag{34}$$

k, **K**, and **N** are *not* an orthogonal basis set, as $\mathbf{k} \cdot \mathbf{K} = \cos\theta$. Combining (32) and (33) gives

$$-C\sin\theta\theta' = [\mathbf{K} \cdot \mathbf{\Gamma} - \mathbf{k} \cdot \mathbf{\Gamma}\cos\theta]/w - C\mu\sin i\sin\theta\sin\phi. \tag{35}$$

Equations (32), (34), and (35) govern the evolution of the magnitude and orientation of the satellite's spin vector.

7.1. *Solid Body Torque*

The instantaneous torque exerted by the planet on the permanent figure of the satellite is given by MacCullagh's formula:

$$\mathbf{\Gamma}_1 = \frac{3Gm_p}{r^5}[(C - B)(\mathbf{r} \cdot \mathbf{j})(\mathbf{r} \cdot \mathbf{k})\mathbf{i} + (A - C)(\mathbf{r} \cdot \mathbf{k})(\mathbf{r} \cdot \mathbf{i})\mathbf{j} + (B - A)(\mathbf{r} \cdot \mathbf{i})(\mathbf{r} \cdot \mathbf{j})\mathbf{k}], \tag{36}$$

where $A \le B \le C$ are the principal moments of inertia associated with the axes **i**, **j**, and **k**, respectively. In order to average this torque over both an orbital period and one rotation of the satellite, we write **r** and the unit vectors **i**, **j**, and **k** in terms of the mutually orthogonal vectors **K**, **N**, and $\mathbf{M} \equiv \mathbf{K} \times \mathbf{N}$. For a circular orbit, the longitude of the planet measured from the **I** direction, λ, increases linearly with time and the planet's position is given by

$$\mathbf{r} = r(\cos f\mathbf{N} + \sin f\mathbf{M}), \tag{37}$$

where $f \equiv \lambda - \phi$. The principal axes are given by the expressions

$$\begin{aligned}\mathbf{i} &= \cos\psi\mathbf{N} + \sin\psi\cos\theta\mathbf{M} + \sin\psi\sin\theta\mathbf{K}\\ \mathbf{j} &= -\sin\psi\mathbf{N} + \cos\psi\cos\theta\mathbf{M} + \cos\psi\sin\theta\mathbf{K}\\ \mathbf{k} &= -\sin\theta\mathbf{M} + \cos\theta\mathbf{K}.\end{aligned} \tag{38}$$

Substituting the above expressions into (36), forming the scalar products $\mathbf{\Gamma}_1 \cdot \mathbf{k}$, $\mathbf{\Gamma}_1 \cdot \mathbf{K}$, and $\mathbf{\Gamma}_1 \cdot \mathbf{N}$, and then conducting a partial averaging over complete cycles of ψ and λ, at constant values of θ and ϕ, we obtain after considerable algebra (checked using the computer algebra package MACSYMA) the desired average torque components,

$$\begin{aligned}\langle\mathbf{\Gamma}_1 \cdot \mathbf{k}\rangle &= \langle\mathbf{\Gamma}_1 \cdot \mathbf{K}\rangle\\ &= -\frac{3Gm_p}{8\mathbf{r}^3}(B - A)(1 + \cos\theta)^2\langle\sin 2(\psi - f)\rangle\end{aligned} \tag{39}$$

and

$$\begin{aligned}\langle\mathbf{\Gamma}_1 \cdot \mathbf{N}\rangle = &-\frac{3Gm_p}{8r^3}(B - A)\sin\theta(1 + \cos\theta)\langle\cos 2(\psi - f)\rangle\\ &-\frac{3Gm_p}{2r^3}[C - (B + A)/2]\sin\theta\cos\theta,\end{aligned} \tag{40}$$

where the $\langle\,\rangle$ notation denotes a time average we have not taken, and will not take, for the following reason. For non-synchronous rotation $\psi' - f' \simeq w - n$, where n is the orbital mean motion, so that $\sin 2(\psi - f)$ and $\cos 2(\psi - f)$ average to zero, and there is no contribution from the terms proportional to $B - A$ to the average torque. However, as the satellite nears a state of synchronous rotation, $\psi' - f'$ goes to zero and these terms turn on. Eventually the torque associated with these terms acts to stabilize the synchronous rotation state (Goldreich and Peale 1966). For simplicity, we write

$$\psi_0 \equiv \psi - f = \psi + \phi - \lambda, \tag{41}$$

where ψ_0 becomes constant for synchronous rotation. Geo-

metrically, ψ_0 is the broken angle between the satellite's minimum moment of inertia axis (**i**) and the direction to the planet, broken at the ascending node. We must stress that ψ_0 is *not* just the Euler angle locating the long axis.

The component of $\langle \boldsymbol{\Gamma}_1 \cdot \mathbf{N} \rangle$ proportional to $C - (A + B)/2$ is the usual torque responsible for the precession of the spin axis of the satellite about the orbit normal, and is independent of the rotation rate.

Finally, we may combine the above expressions for the torque components to write a complete expression for the average solid-body torque,

$$\langle \boldsymbol{\Gamma}_1 \rangle = -CR(1 + \cos\theta)\sin 2\psi_0[\mathbf{k} + \mathbf{K}] - [CR\sin\theta(1 + \cos\theta)\cos 2\psi_0 + CS\sin\theta\cos\theta]]N, \tag{42}$$

where we have introduced the shorthand notations

$$R \equiv \frac{3Gm_p}{8r^3}\frac{B - A}{C} \tag{43}$$

and

$$S \equiv \frac{3Gm_p}{2r^3}\frac{C - (B + A)/2}{C}. \tag{44}$$

Both R and S are angular accelerations due to the planetary torque on the satellite's solid body deformations. Torques containing the coefficient R (which is proportional to the triaxiality) can be seen to average out in a complete ψ_0 cycle (if θ is roughly constant during that cycle). S is the angular acceleration exerted due to the oblateness of the satellite; the precession induced by this torque primarily affects the ϕ variable.

7.2. *Tidal Torque*

The planet exerts an additional torque on the satellite due to the phase lag in the tidal bulge it raises. Goldreich and Peale (1968) give expressions for the components of the tidal torque, $\boldsymbol{\Gamma}_2 \cdot \mathbf{k}$ and $\boldsymbol{\Gamma}_2 \cdot \mathbf{K}$, in terms of sums over components in the Fourier expansion of the tidal potential due to Kaula (1964). Even for zero eccentricity, however, the resulting expressions are rather lengthy. A more direct, physical approach is to modify the MacDonald (1964) tide formalism, in which the tidal bulge is modeled as a hydrostatic equilibrium tide which lags the tide-raising potential by a constant angle, δ. Instead of fixing δ, which is somewhat unphysical, we assume a constant tidal time lag, Δt. This particular formalism, also known as the "frequency-dependent" tide model in the context of the Kaula expansion, has the added virtue for our current purposes that the angular phase lag goes smoothly to zero for synchronous rotation, and reverses sign for sub-synchronous rotation. In terms of the usual tidal dissipation factor Q, the tidal phase lag $2(w - n)\Delta t \simeq 1/Q$ (Goldreich and Peale 1970).

Denoting the retarded position of the planet relative to the satellite *in body-fixed coordinates* by $\boldsymbol{\rho}$, the tidal torque is then given by (Goldreich and Peale 1970)

$$\boldsymbol{\Gamma}_2 = \frac{3k_2Gm_p^2R_s^5}{r^6}\frac{(\mathbf{r}\cdot\boldsymbol{\rho})\boldsymbol{\rho}\times\mathbf{r}}{\rho^2 r^2}, \tag{45}$$

where k_2 is the satellite's second-order Love number and R_s is the satellite's mean radius. Allowing for both the orbital and rotational motion during the interval Δt, we find

$$\boldsymbol{\rho} \simeq \mathbf{r} - (n\mathbf{K}\times\mathbf{r})\Delta t + (w\mathbf{k}\times\mathbf{r})\Delta t. \tag{46}$$

Writing $\mathbf{r} = r(\cos\lambda\mathbf{I} + \sin\lambda\mathbf{J})$, and using Eq. (29), we have

$$(\boldsymbol{\rho}\times\mathbf{r})/r^2 = w\,\Delta t[\sin\theta\sin\phi\cos\lambda - \sin\theta\cos\phi\sin\lambda]\hat{\mathbf{r}} - w\,\Delta t\,\mathbf{k} + n\,\Delta t\,\mathbf{K}. \tag{47}$$

For $w\,\Delta t \ll 1$ and $n\,\Delta t \ll 1$, $\boldsymbol{\rho}\cdot\mathbf{r} \simeq r^2$. Averaging the resulting expression for $\boldsymbol{\Gamma}_2$ over an orbit, we then obtain

$$\langle \boldsymbol{\Gamma}_2 \rangle = -\frac{CT}{2}[w\mathbf{k} + (w\cos\theta - 2n)\mathbf{K}], \tag{48}$$

where

$$T \equiv \frac{3k_2Gm_p^2R_s^5}{Cr^6}\Delta t. \tag{49}$$

For $w \gg n$ and small θ, wT can be identified as the satellite's tidal angular deceleration rate (*c.f.* Eq. (9)). Finally, we evaluate the scalar products

$$\langle \boldsymbol{\Gamma}_2 \cdot \mathbf{k} \rangle = -\frac{CT}{2}[2w - w\sin^2\theta - 2n\cos\theta] \tag{50}$$

and

$$\langle \boldsymbol{\Gamma}_2 \cdot \mathbf{K} \rangle = -\frac{CT}{2}[2w\cos\theta - 2n]. \tag{51}$$

Clearly, $\langle \boldsymbol{\Gamma}_2 \cdot \mathbf{N} \rangle = 0$. The latter expressions may also be derived from those given by Goldreich and Peale (1968) for $e = 0$, by assuming that their individual Fourier component phase lags, $\varepsilon_{mpq} = \sigma_{mpq}\,\Delta t$, where the σ_{mpq} are the tidal component frequencies.

7.3. Equations of Motion

We substitute expressions (39), (40), (50), and (51) for the solid body and tidal torque components into Eqs. (32), (34), and (35) to obtain the final orbit-averaged equations of motion:

$$w' = -T\left[w\left(1 - \frac{1}{2}\sin^2\theta\right) - n\cos\theta\right] - R(1 + \cos\theta)^2 \sin 2\psi_0 \tag{52}$$

$$\theta' = \mu \sin i \sin\phi + T\sin\theta\left[\frac{1}{2}\cos\theta - \frac{n}{w}\right] + \frac{R}{w}[\sin\theta(1 + \cos\theta)]\sin 2\psi_0 \tag{53}$$

$$\phi' = \mu[\sin i \cot\theta \cos\phi + \cos i] - \frac{S}{w}\cos\theta - \frac{R}{w}(1 + \cos\theta)\cos 2\psi_0. \tag{54}$$

For non-synchronous rotation, $\langle \sin 2\psi_0 \rangle = \langle \cos 2\psi_0 \rangle = 0$ and Eqs. (52), (53), and (54) form a complete set. For rotation near the synchronous rate we also need an equation for ψ_0'. Starting with the elementary expression for the rotational angular velocity relative to inertial space

$$\mathbf{w} = \phi'\mathbf{K} + \theta'\mathbf{N} + \psi'\mathbf{k} - \mu\mathbf{n},$$

we obtain for the component of angular velocity about the C axis

$$w_c = \psi' + \phi'\cos\theta + \mu(\sin i \cos\phi \sin\theta - \cos i \cos\theta).$$

This expression is identical to that given by Peale (1974), as Eq. (9). Now, the satellite's sidereal mean motion, for small orbital inclination, is

$$n \simeq \lambda' - \mu$$

so we have, from Eq. (41),

$$\psi_0' = \psi' + \phi' - \lambda' = w - n + \phi'(1 - \cos\theta) - \mu(1 - \cos i \cos\theta + \sin i \cos\phi \sin\theta),$$

where we have assumed that $w_c = w$ (*i.e.*, principal axis rotation). In fact, we will use the simpler approximate expression

$$\psi_0' \simeq w - n, \tag{55}$$

where the neglected terms of $\mathcal{O}(\phi')$ and $\mathcal{O}(\mu)$ are generally small compared with $w - n$, and are of the same size as the off-axis components w_a and w_b which have already been neglected by our initial assumption of principal axis rotation.

7.4. Non-dimensionalization

We switch to a dimensionless set of variables via the following transformations:

$$\tau = \mu t, \quad \omega = \frac{\mu}{S}w, \quad \gamma = \frac{\mu}{S}n$$
$$\alpha = S/\mu^2, \quad \beta = \frac{R}{S}, \quad \varepsilon = T/\mu. \tag{56}$$

The angles θ, ϕ, and ψ_0 are unchanged. However, the dimensionless spin rate ω and mean motion γ are expressed not in units of μ ($1/\mu$ being the dimensionless time unit), but in units of S/μ. This quantity is, to within a factor of cos θ, the precessional acceleration of the satellite (in inertial space) due to the oblateness torque in one time unit. When these substitutions are made, the dimensionless equations of motion (3)–(6) result.

8. APPENDIX B

In an attempt to explain the instability of S_2, we linearize Eqs. (3)–(6) around an equilibrium point, say (ψ_{eq}, ω_{eq}, θ_{eq}, ϕ_{eq}), to obtain the first variational equations on ($\delta\psi_0$, $\delta\omega$, $\delta\theta$, $\delta\phi$). We find the following equation governing the evolution of $\delta\theta$:

$$\dot{\delta\theta} = \left\{\frac{2\beta}{\gamma}\sin\theta_{eq}(1 + \cos\theta_{eq})\cos 2\psi_{eq}\right\}\delta\psi_0 + \{\sin i \cos\phi_{eq}\}\,\delta\phi + \left\{\frac{\varepsilon}{\gamma}\sin\theta_{eq} - \frac{\beta}{\gamma^2}\sin\theta_{eq}(1 + \cos\theta_{eq})\sin 2\psi_{eq}\right\}\delta\omega + \left\{\frac{\varepsilon}{2}(2\cos\theta_{eq} + 1)(\cos\theta_{eq} - 1) + \frac{\beta}{\gamma}(2\cos\theta_{eq} - 1)(\cos\theta_{eq} + 1)\sin 2\psi_{eq}\right\}\delta\theta.$$

However, (24) requires that ψ_{eq} is small, of $\mathcal{O}(\varepsilon\gamma/\beta)$ and we assume that sin $i \ll \beta/\gamma$. As a result, when compared to the coefficient of $\delta\psi_0$, which is of $\mathcal{O}(\beta/\gamma)$, the remaining coefficients are small in the above equation (we are assuming that sin $i \ll 1$). Consequently, we neglect all terms in this variational equation, except that of $\delta\psi_0$.

Under these conditions, the variational equation for $\delta\phi$ decouples; $\delta\phi$ does not appear in the equations governing $\delta\psi_0$ or $\delta\omega$, and we have neglected its appearance in the equation governing $\delta\theta$. This leads to the system

$$\delta\dot{\theta} = \left\{\frac{2\beta}{\gamma}\sin\theta_{eq}(1+\cos\theta_{eq})\cos 2\psi_{eq}\right\}\delta\psi_0,$$

$$\delta\dot{\psi}_0 = \alpha\,\delta\omega,$$

$$\begin{aligned}\delta\dot{\omega} = &-\{2\beta(1+\cos\theta_{eq})^2\cos 2\psi_{eq}\}\,\delta\psi_0 \\ &-\left\{\frac{\varepsilon}{2}(1+\cos^2\theta_{eq})\right\}\delta\omega - \{\varepsilon\gamma\sin\theta_{eq}(1-\cos\theta_{eq}) \\ &-2\beta\sin\theta_{eq}(1+\cos\theta_{eq})\sin 2\psi_{eq}\}\,\delta\theta,\end{aligned} \tag{57}$$

which is simply a linear, third-order, constant-coefficient ordinary differential equation, approximating the evolution near a high obliquity equilibrium point. The eigenvalues of this system (zeros of a third-order polynomial) are easily computed, and, in fact, can be found in closed form. However, the calculations quickly become unwieldy, even when using computer algebra systems such as MACSYMA or Maple. In addition, the coefficients depend on the locations of the equilibrium points, which must be determined numerically.

Using the numerically obtained locations of the equilibrium points on S_2, we find that, as hoped, Eqs. (57) are unstable for small γ and stable for large γ, just as are the full triaxial equations (see Figs. 9 and 10). At the transition between stability and instability of S_2, these simplified equations possess one negative real eigenvalue and a pair of purely imaginary eigenvalues. This indicates the existence of a Hopf bifurcation in Eqs. (57) and results in the change of stability along this branch of equilibria (along with additional minor conditions which are satisfied; see Guckenheimer and Holmes 1983). As a final calculation we find the location at which S_2 changes stability; specifically, we locate the points at which there exists a pair of purely imaginary eigenvalues. A general third-order polynomial $\lambda^3 + c_2\lambda^2 + c_1\lambda + c_0 = 0$ has a pair of purely imaginary roots if $c_0 = c_1c_2$. Subsequently obtaining the characteristic polynomial of Eqs. (57) and satisfying the above relationship, we find that our requirement of pure imaginary eigenvalues is satisfied if

$$\begin{aligned}&\varepsilon\gamma\{\cos^2\theta_{eq} - 4\cos\theta_{eq} + 1\} \\ &\quad - 4\beta\sin^2\theta_{eq}\sin 2\psi_{eq} = 0.\end{aligned} \tag{58}$$

Using (24) to obtain the equilibrium value of $\sin 2\psi_{eq}$, surprisingly we find that (58) reduces to an expression with *no* parameter dependence,

$$\cos^3\theta_{eq} - 3\cos^2\theta_{eq} + 9\cos\theta_{eq} - 3 = 0,$$

which can be solved for θ_{eq} to yield

$$\begin{aligned}\theta_{eq} &= \arccos\left\{-(2+2\sqrt{3})^{1/3} + \frac{2}{(2+2\sqrt{3})^{1/3}} + 1\right\} \\ &= 1.187 \equiv \theta_{cr} \simeq 68°.\end{aligned} \tag{59}$$

As a result of this unexpected simplification, our branch of solutions changes stability when $\theta_{eq} > \theta_{cr}$ *independent of the parameters*. However, the location of the bifurcation in ψ_0, ω, and ϕ does depend on the parameter values.

Because of the neglected terms in Eqs. (57), this result is expected to carry over only approximately to the full set of Eqs. (3)–(6). However, noting Figs. 9 and 10, we find good agreement between the location of the Hopf bifurcation and θ_{cr}. We find that as the remaining parameters are varied, the location of the bifurcation is constant in θ to several significant figures (although the other state variables will change). Observe that exactly the same analysis carries through for S_4, resulting in the same value of θ_{cr}, but this does not affect the overall stability of the fixed point since the positive real root (contained in the ϕ variational equation) is always present above and below the Hopf bifurcation. In summary, if a satellite has a value of γ which results in there existing fixed points at obliquities that have $\theta > \theta_{cr}$, then these fixed points will be unstable.

ACKNOWLEDGMENTS

This paper is the outgrowth of several semester projects in dynamics over 4 years at Cornell, and we acknowledge the encouragement of Professors Phil Holmes and Joe Burns of the T&AM department. We have benefited greatly from an extended dialogue with Stan Peale of UCSB, whose original work on Mercury stimulated this investigation and who also independently checked the derivations in Appendix A. Greg Black contributed considerable insight into the reliability of the averaged equations by providing comparisons with integrations of the full Euler equations. Peter Thomas provided the data on satellite shapes used for the calculations of the dimensionless parameters. Jihad Touma (as a reviewer) and Don Banfield made suggestions which improved the conciseness of the paper. This work was supported by NASA Grants NAGW-310 and NAGW-544.

REFERENCES

Beletskii, V. V. 1972. Resonance rotation of celestial bodies and Cassini's Laws. *Celest. Mech.* **6**, 356–378.

Burns, J. A. 1977. Orbital Evolution. In *Planetary Satellites* (J. A. Burns, Ed.), pp. 113–156. Univ. Arizona Press, Tucson.

Burns, J. A., and V. S. Safronov 1973. Asteroid nutation angles. *Mon. Not. R. Astron. Soc.* **165**, 403–411.

Colombo, G. 1966. Cassini's second and third laws. *Astron. J.* **71**, 891–896.

Darwin, G. H. 1879. On the precession of a viscous spheroid and on the remote history of the earth. *Phil. Trans. R. Soc. London* **170**, 447–530.

DERMOTT, S. F., AND P. C. THOMAS 1988. The shape and internal structure of Mimas. *Icarus* **73**, 25–65.

DICKEY, J. O., and 11 colleagues. 1994. Lunar laser ranging: A continuing legacy of the Apollo program. *Science* **265**, 482–490.

GOLDREICH, P. 1966a. Final spin states of planets and satellites. *Astron. J.* **71**, 1–7.

GOLDREICH, P. 1966b. History of the lunar orbit. *Rev. Geophys.* **4**, 411–439.

GOLDREICH, P., AND S. J. PEALE 1966. Spin-orbit coupling in the solar system. *Astron. J.* **71**, 425–438.

GOLDREICH, P., AND S. J. PEALE 1968. The dynamics of planetary rotations. *Ann. Rev. Astron. Astrophys.* **6**, 287-320.

GOLDREICH, P., AND S. J. PEALE 1970. The obliquity of Venus. *Astron. J.* **75**, 273–284.

GUCKENHEIMER, J. AND P. HOLMES 1983. *Nonlinear Oscillations, Dynamical Systems, and Bifurcations of Vector Fields*. Springer-Verlag, New York.

HARRIS, A. W. 1994. Tumbling asteroids. *Icarus* **107**, 209–211.

HENRARD, J., AND C. MURIGANDE 1987. Colombo's top. *Celest. Mech.* **40**, 345–366.

HOLDEN, LISA, AND T. ERNEUX 1993. Understanding bursting oscillations as periodic slow passages through bifurcation and limit points. *J. Math. Biol.* **31**, 351–365.

JANKOWSKI, D. B., C. F. CHYBA, AND P. D. NICHOLSON 1989. On the obliquity and tidal heating of Triton. *Icarus* **80**, 211–219.

KADONA, T. 1993. Change in spin orientation of satellites by an oblique impact. *Icarus* **105**, 580-584.

KAULA, W. M. 1964. Tidal dissipation by solid friction and the resulting orbital evolution. *Rev. Geophys.* **2**, 661–685.

LISSAUER, J. J. 1985. Can cometary bombardment disrupt synchronous rotation of planetary satellites? *J. Geophys. Res.* **90**, 11289–11293.

MACDONALD, G. J. F. 1964. Tidal friction. *Rev. Geophys.* **2**, 467–541.

PEALE, S. J. 1969. Generalized Cassini's laws. *Astron. J.* **74**, 483–489.

PEALE, S. J. 1973. Rotation of solid bodies in the solar system. *Rev. Geophys. Space Phys.* **11**, 767–793.

PEALE, S. J. 1974. Possible histories of the obliquity of Mercury. *Astron. J.* **79**, 722–744.

PEALE, S. J. 1977. Rotation histories of the natural satellites. In *Planetary Satellites*, (J. A. Burns, Ed.), pp. 87–112. Univ. Arizona Press, Tuscon.

QUINN, D. D. 1995. *Resonance Capture in Dynamical Systems.* Ph.D. Thesis, Cornell University.

RUBINCAM, D. P., B. F. CHAO, AND P. C. THOMAS 1995. The gravitational field of Deimos. *Icarus* **114**, 63–67.

THOMAS, P. C. 1988. Radii, shapes, and topography of the satellites of Uranus from limb coordinates. *Icarus* **73**, 427–441.

THOMAS, P. C., AND S. F. DERMOTT 1991. The shape of Tethys. *Icarus* **94**, 391–398.

THOMAS, P. C. 1991. *Planetary Geodesy. Reviews of Geophys., Suppl.* U.S. National Report to IUGG 1987–1990, pp. 182–187.

WARD, W. 1975. Past orientation of the lunar spin axis. *Science* **189**, 377–379.

WARD, W. 1981. Orbital inclination of Iapetus and the rotation of the Laplacian plane. *Icarus* **46**, 97–107.

WIDSOM, J. 1987. Rotational dynamics of irregularly shaped natural satellites. *Astron. J.* **94**, 1350–1360.

YODER, C. F. 1995. Astrometric and geodetic properties of Earth and the Solar System. In *Global Earth Physics: A Handbook of Physical Constants*, AGU Reference Shelf 1.